EFFECT OF METAL OXIDE-SUBSTITUTED LACOO$_3$ PEROVSKITE SUPPORT
ON THE CATALYTIC PROPERTIES OF NI/PEROVSKITE IN CARBON
DIOXIDE REFORMING OF METHANE

By
MISS Phakampai AUNMUNKONG

A Thesis Submitted in Partial Fulfillment of the Requirements
for Doctor of Engineering (CHEMICAL ENGINEERING)
Department of CHEMICAL ENGINEERING
Graduate School, Silpakorn University
Academic Year 2018
Copyright of Graduate School, Silpakorn University

ผลของตัวรองรับแลนทานัมโคบอลไทต์เพอรอฟสไกต์ ที่ถูกแทนด้วยโลหะออกไซด์ ต่อ
สมบัติการเร่งปฏิกิริยาของนิกเกิลบนเพอรอฟสไกต์ ในการรีฟอร์มมิ่งมีเทนด้วย
คาร์บอนไดออกไซด์

โดย
นางสาวพักตร์อำไพ อั้นมั่นคง

วิทยานิพนธ์นี้เป็นส่วนหนึ่งของการศึกษาตามหลักสูตรวิศวกรรมศาสตรดุษฎีบัณฑิต
สาขาวิชาวิศวกรรมเคมี แบบ 1.1 ระดับปริญญาดุษฎีบัณฑิต
ภาควิชาวิศวกรรมเคมี
บัณฑิตวิทยาลัย มหาวิทยาลัยศิลปากร
ปีการศึกษา 2561

EFFECT OF METAL OXIDE-SUBSTITUTED LACOO₃ PEROVSKITE
SUPPORT ON THE CATALYTIC PROPERTIES OF NI/PEROVSKITE
IN CARBON DIOXIDE REFORMING OF METHANE

By

MISS Phakampai AUNMUNKONG

Title	EFFECT OF METAL OXIDE-SUBSTITUTED LaCoO$_3$ PEROVSKITE SUPPORT ON THE CATALYTIC PROPERTIES OF Ni/PEROVSKITE IN CARBON DIOXIDE REFORMING OF METHANE
By	Phakampai AUNMUNKONG
Field of Study	(CHEMICAL ENGINEERING)
Advisor	CHOOWONG CHAISUK

Graduate School Silpakorn University in Partial Fulfillment of the Requirements for the Doctor of Engineering

.... Dean of graduate school
(Associate Professor Jurairat Nunthanid, Ph.D.)

Approved by

.... Chair person
(Assistant Professor VEERAYUT LERSBAMRUNGSUK , D.Eng.)
.... Advisor
(Assistant Professor CHOOWONG CHAISUK , D.Eng.)
.... Examiner
(Assistant Professor OKORN MEKASUWANDUMRONG , D.Eng.)
.... External Examiner
(Professor Navadol Laosiripojana , Ph.D.)
.... External Examiner
(Thana Sornchamni , Ph.D.)
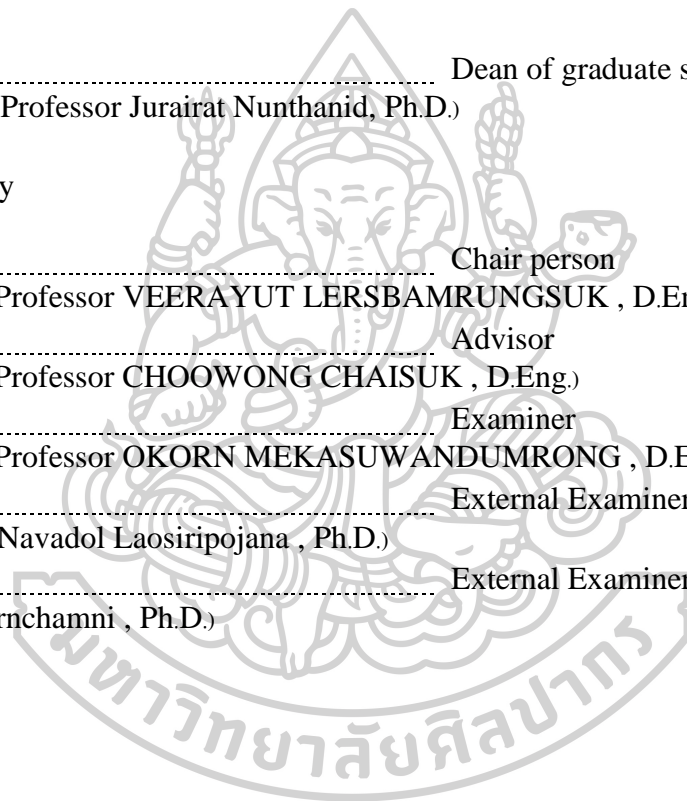
56404802 : Major (CHEMICAL ENGINEERING)

MISS PHAKAMPAI AUNMUNKONG : EFFECT OF METAL OXIDE-SUBSTITUTED LACOO₃ PEROVSKITE SUPPORT ON THE CATALYTIC PROPERTIES OF NI/PEROVSKITE IN CARBON DIOXIDE REFORMING OF METHANE THESIS ADVISOR : ASSISTANT PROFESSOR CHOOWONG CHAISUK, D.Eng.

The effect of the Ni loading on the $LaCoO_3$ perovskites, the Ce substitution into La position and the transition metal (Cu, Mn and Zn) substitution into Co position on the $LaCoO_3$ perovskites structure in Ni/perovskites catalysts was investigated. First, the $LaCoO_3$ perovskites (LC) were prepared by flame spray pyrolysis (FSP), and then the xNi (x = 0, 2, 5 and 10 wt%) was loaded by incipient wetness impregnation method. The catalysts were investigated using a quartz tubular reactor under the atmospheric pressure of 700 ºC for 15h. The Ni loading maintains the perovskite structure. The 2Ni/LC shows the highest reducibility and intensity in the $La_2O_2CO_3$ phase. The LC catalyst was inactive due to the reduction temperature to 500 ºC which was not enough to produce the Co metal dispered in the La_2O_3 support. The 2Ni/LC catalyst showed the highest CH_4 and CO_2 conversions and H_2/CO ratio and stability for the 15 h conversion. When increasing the Ni loading by 5 and 10 wt%, the CH_4 conversion decreases due to the RWGS reaction which is favored a Ni-enriched surface found on the perovskite support. And then, the $2Ni/Ce_xLa_{1-x}CoO_3$ (x = 0.0, 0.2, 0.4, 0.6, 0.8 and 1.0) were investigated. The Ce contents x = 0.2, was inserted into the perovskite structure. When increasing Ce more than 0.2 ratio, it appears segregated in the CeO_2 phase. CeO_2 can provide the stabilization of lattice oxygen O_2 on the surface which it gave the high catalytic activity and stability after the initial 3 hours. The substitution of the La site metal ion with Ce metal ion at x = 0.2, 0.4 and 0.6 show little change in the CO_2 and CH_4 conversion. At x=0.8 and 1.0, it shows an increase in the CO_2 conversion and CO yield due to the effect of RWGS reaction. Its insertion in the perovskite structure is also possible in the low Ce-content. Finally, the transition metal (Cu, Mn and Zn) substitution into Co position were investigated. The perovskite structures were formed when using Co and Mn metals but they did not forme when using Zn and Cu metal. All of the Mn/Co ratio maintains the perovskite structure. The Mn/Co ratio at 0.05 shows the highest CH_4 conversion, H_2 yield and H_2/CO ratio. The Mn and Co mix metals increase catalytic activity due to a change in oxygen mobility within the crystal lattice of the Co component. The Mn/Co ratio at 0.1-0.5 show a decrease in the CO_2 and CH_4 conversion after the 9 hr mark due to metals sintering.

ACKNOWLEDGEMENTS

I would like to thank you very much for my dissertation advisor, Assistant Professor Choowong Chaisuk for his useful suggestions and discussions throughout the course of this research. Not only this research, he also many other methodologies in life. This dissertation would not have been completed if I did not have support from him.

In addition, I would like to thank Synchorotron Light Research Institute for the characterize support (XPS and XAS technique) and grateful for the kind cooperation from Assistant Professor Veerayut Lersbamrungsuk as the chair person, Assistant Professor Okorn Mekasuwandumrong as the examiner, Professor Navadol Laosiripojana and Dr. Thana Sornchamni as the external examiner of the dissertation committee.

Finally, I would like to express my sincere thanks to my parents, my friends and my english teacher for their suggestions and help.
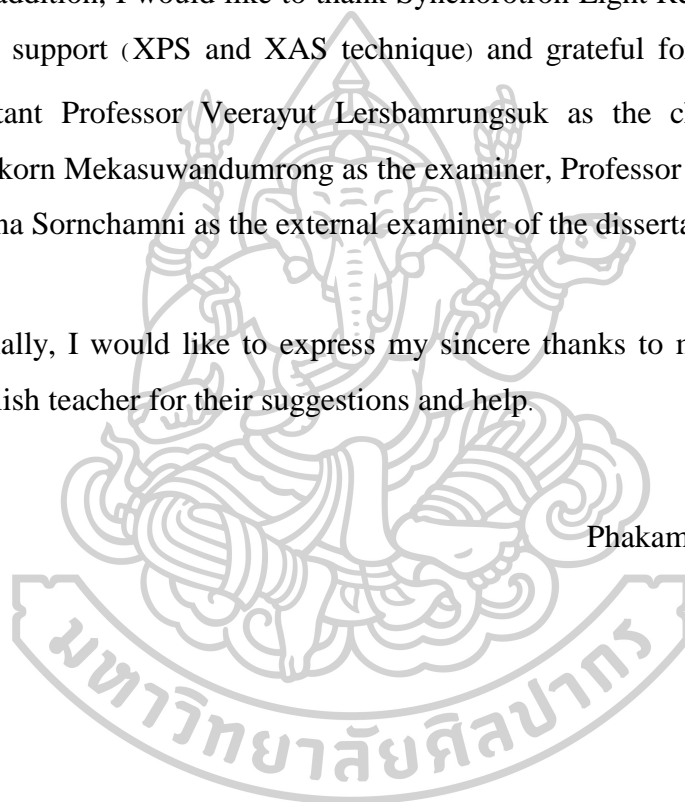
Phakampai AUNMUNKONG

TABLE OF CONTENTS

LIST OF FIGURES

LIST OF TABLES

CHAPTER I
INTRODUCTION

Currently, the excessive use of natural gas and fossil fuels by rapidly industrial plants causes greenhouse gas, which include methane gas (CH_4), carbon dioxide (CO_2), nitrogen oxides (NO_x), ozone (O_3) and others. The major greenhouse gases are CO_2 and CH_4. By this reason, the carbon dioxide reforming of methane, known as dry reforming of methane (DRM) attracts interest because both CH_4 and CO_2 are readily available reactants. DRM not only helps in decreasing toxic airborne emissions, but it also allows for the production of syngas (CO/H_2). This syngas is the starting point of methanol synthesis and a raw material used in the Fischer-Tropsch synthesis (FTS) [1, 2].

The studies on catalysts for DRM reaction are divided into 2 groups, noble and transition metals [1]. In the case of noble metal catalysts, such as Pt, Pd and Ru, they have been shown to exhibit high activity in methane and less sensitive to coking. However, the economy view, the noble metals aren't suitable upscale for industrial level due to their high cost and restricted availability. On the other hand, the transition metals, such as Fe, Co and Ni based catalysts is commonly studied due to its low cost, stability and better availability. They show high activity but rapidly deactivate [3, 4]. However, the major problem in this reaction is the accumulation of carbon on the surface of the catalysts and sintering of the active site, resulting in catalyst deactivation [5].

Furthermore, the coke formation on the surface is to be remedied especially for Ni metal catalyst. The catalytic activity and stability of the nickel catalyst is effected by many factors such as nickel dispersion, basic supports, redox promoters, conditions for the catalysts preparation and the chemical interaction between nickel and the support [6]. This last factor occurs when nickel display disperses into well such as perovskite, spinel and fluorite. The reduction size of the Ni particles leads to a homogeneously distribution and small metal nanoparticles, which inhibits coke formation and enhances catalytic stability [7-9].

Perovskite-type oxides structures are general formula ABO_3. At site A there are lanthanides, such as Ce and La. At site B there are transition metals such as Fe, Co, Mn, Zn, etc. This structure shows particular promise for applications relating to high temperatures and high stability. In addition, partial replacement at the B sites can increase catalytic activity due to a change in oxygen mobility within the crystal lattice of the B component [10]. Another advantage of this structure, it can be added to a noble

metal by impregnation from an aqueous solution in preparation of the oxide support and partial substitution at A and B sites [11].

The $LaCoO_3$ perovskite invokes particular interest because it has versatile structures (ABO_3-type perovskites) and is produce in several methods such as solvothermal, sol-gel and flame spray pyrolysis (FSP)[12]. It is a major challenge for perovskites to suppress carbon formation maintain high thermal stability and to inhibit the sintering of the metal [13]. The catalyst formed after $LaCoO_3$ reduction showed high Co metal dispersion with La_2O_3-supported, which can react with the reactant of CO_2, with lead to $La_2O_2CO_3$ formation. It gave high activities and stabilities[14]. One way to prepare this structure is the flame spray pyrolysis (FSP). It can offer a continuous one-step production of a high intensity crystalline particle and creates high BET surface areas. Several studies have investigated the preparation of supported metal by this method [15-17].

A procedure to improve the activity and stability of $LaCoO_3$ is introducing structural modifications in the perovskite by partial substitution of Co site by other transition metals (Zn, Cu, Fe, Cr, Mn, etc). In addition, the La site was substituted by Ca or Sr are resistant to coke deposition in dry reforming[18, 19]. CeO_2 can provide the stabilization of lattice oxygen O_2 on the surface which gave it the high catalytic activity and stability [4]. Lima et al.[20] studied the effect of the Ce partial substitution into La position. The $La_{1-x}Ce_xNiO_3$ catalyst (x = 0.00, 0.05, 0.04, and 0.70) were tested by DRM. This low amount (x = 0.05) are shown incorporation with perovskite structure confirm by XRD results. It shown the highest CH_4 and CO_2 conversion and stability. Gustavo et al.[21] investigated on the development perovskite catalysts. The $LaNi_{1-x}Mn_xO_3$ (x = 0.0, 0.2, 0.4, 0.6, 0.8 and 1.0) catalysts were prepared by sol-gel method and tested in the DRM reaction. It was observed that the reduction step increases the Ni^{3+} to Ni^o lead to Ni metal on MnO_x-La_2O_3 support. The catalysts at x $\leq$ 0.8 showed high activity and H_2/CO ratio due to the Ni metal disperse on $La_2O_2CO_3$-MnO-Mn_2O_3 phases, which it confirm the XRD signal of spent catalyst. These phase corresponds to high activity and stability.

In this work, the $LaCoO_3$ perovskites were prepared by flame spray pyrolysis (FSP), and then the Ni was loaded by incipient wetness impregnation method. We have studied effect of Ni loading, the Ce partial substitution into La position and the transition metal (Cu, Mn, Zn) substitution into Co position on the catalytic performance of Ni/$LaCoO_3$ based catalysts in the carbon dioxide reforming of methane.

1.1 Objective of research

The purpose of this work is to study effect of metal-substituted $LaCoO_3$ perovskite support on the catalytic properties of Ni/perovskite in carbon dioxide reforming of methane.

1.2 Scope of research

Scope of this work is divided into three parts.

1.2.1 Effect of Ni loading on the $LaCoO_3$ perovskites

The $LaCoO_3$ perovskites are prepared by flame spray pyrolysis (FSP) and Ni is loaded by incipient wetness impregnation method. The nickel loading is varied at 0, 2, 5 and 10 wt%.

1.2.2 Effect of Ce partial substitution into La position

The appropriate nickel loading is selected. The La was substituted by Ce and the perovskite structure becomes $Ni/Ce_xLa_{1-x}CoO_3$ (x = 0, 0.2, 0.4, 0.6, 0.8 and 1.0)

1.2.3 Effect of the transition metal substitution into Co position

The appropriate nickel loading is selected. The Co position was substituted by the transition metal (Mn, Zn and Cu). Finally, the transition metals (B=Mn, Zn and Cu) was selected and it partially substituted each into the Co position which resulted in $Ni/LaB_yCo_{1-y}O_3$ (y=0, 0.05, 0.1, 0.5, and 1.0).

All catalysts were characterized and evaluated. The bulk crystal structure and chemical phase composition are determined by X-ray diffraction (XRD). The BET surface area and pore characteristics of catalysts are determined by N_2 physisorption. Temperature programmed reduction (TPR) is used to determine the reducibility of catalysts. The lanthanum oxide and cerium oxide of the catalysts were analyzed by X-ray photoelectron spectroscopy (XPS) and the X-ray absorption (XAS), which these techniques were using for catalyst part 2. Finally, weight loss rates of catalyst determined by thermogravimetric analysis (TGA).

Lastly, the activity and stability of catalysts are tested by the carbon dioxide reforming of methane. This reaction is occurred in quartz tubular reactor under the atmospheric pressure of 700 $^\circ$C for 15h. The reactant and product are analyzed by GC connecting with TCD detectors.

1.3 Contribution of research

The partial substitution of some metal oxides into La and Co sites on Ni/LaCoO$_3$ perovskite catalysts can improve the activity and stability for the carbon dioxide reforming of methane under atmospheric pressure at 700 $^\circ$C. The perovskites catalysts can promote H$_2$/CO yield ratio nearly 1. This syngas (H$_2$/CO) is a raw material used in the other reaction.
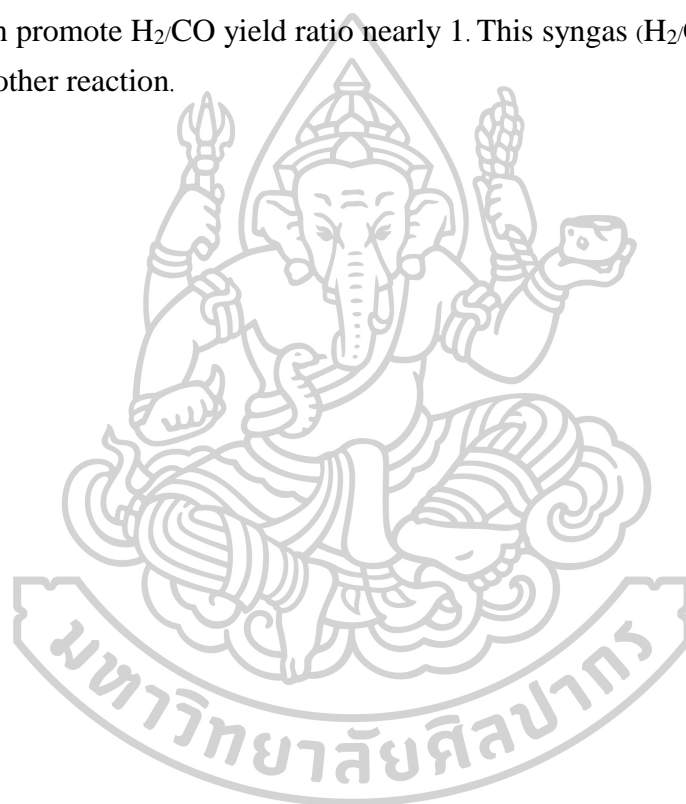
CHAPTER II
BACKGROUND AND LITERATURE REVIEW

2.1 DRM reaction and thermodynamics

The CO_2 reforming of CH_4 or dry reforming of methane (DRM) attracts interest because both CH_4 and CO_2 are inexpensive reactants and it, DRM, produces a syngas (H_2/CO). The DRM also allows for a lower production of syngas ($H_2/CO = 1$), which is the starting point of methanol synthesis and a raw material which is used in the technologies of Fischer-Tropsch synthesis (FTS)[22]. The use of syngas, produced by DRM, has also been considered for the storage of nuclear and solar energy [23]. The main reactions which may occur in DRM are considered in the equation 2.1 and other side reactions as shown in the equations 2.2-2.17.

$$CH_4 + CO_2 \longleftrightarrow 2CO + 2H_2 \qquad \Delta H = 247 \text{ kJ mol}^{-1} \qquad 2.1$$

$$CO_2 + H_2 \longleftrightarrow CO + H_2O \qquad \Delta H = 41 \text{ kJ mol}^{-1} \qquad 2.2$$

$$2CH_4 + CO_2 \longleftrightarrow C_2H_6 + CO + H_2O \qquad \Delta H = 106 \text{ kJ mol}^{-1} \qquad 2.3$$

$$2CH_4 + CO_2 \longleftrightarrow C_2H_4 + 2CO + 2H_2O \quad \Delta H = 284 \text{ kJ mol}^{-1} \qquad 2.4$$

$$C_2H_6 \longleftrightarrow C_2H_4 + H_2 \qquad \Delta H = 136 \text{ kJ mol}^{-1} \qquad 2.5$$

$$CO + 2H_2 \longleftrightarrow CH_3OH \qquad \Delta H = -90.6 \text{ kJ mol}^{-1} \qquad 2.6$$

$$CO_2 + 3H_2 \longleftrightarrow CH_3OH + H_2O \qquad \Delta H = -49.1 \text{ kJ mol}^{-1} \qquad 2.7$$

$$CH_4 \longleftrightarrow C + 2H_2 \qquad \Delta H = 74.9 \text{ kJ mol}^{-1} \qquad 2.8$$

$$2CO \longleftrightarrow C + CO_2 \qquad \Delta H = -172.4 \text{ kJ mol}^{-1} \qquad 2.9$$

$$CO_2 + 2H_2 \longleftrightarrow C + 2H_2O \qquad \Delta H = -90 \text{ kJ mol}^{-1} \qquad 2.10$$

$$H_2 + CO \longleftrightarrow 2H_2O + C \qquad \Delta H = -131.3 \text{ kJ mol}^{-1} \qquad 2.11$$

$$CH_3OCH_3 + CO_2 \longleftrightarrow 3CO + 3H_2 \qquad \Delta H = 258.4 \text{ kJ mol}^{-1} \qquad 2.12$$

$$3H_2O + CH_3OCH_3 \longleftrightarrow 2CO_2 + 6H_2 \qquad \Delta H = 135 \text{ kJ mol}^{-1} \qquad 2.13$$

$$CH_3OCH_3 + H_2O \longleftrightarrow 2CO + 4H_2 \qquad \Delta H = 204.8 \text{ kJ mol}^{-1} \qquad 2.14$$

$$2CH_3OH \longleftrightarrow CH_3OCH_3 + H_2O \qquad \Delta H = -37 \text{ kJ mol}^{-1} \qquad 2.15$$

$$CO_2 + 4H_2 \longleftrightarrow CH_4 + 2H_2O \qquad \Delta H = -165 \text{ kJ mol}^{-1} \qquad 2.16$$

$$CO + 3H_2 \longleftrightarrow CH_4 + H_2O \qquad \Delta H = -206.2 \text{ kJ mol}^{-1} \qquad 2.17$$

Primarily, dry reforming of methane (DRM) is used after steam reforming of methane (SRM). DRM consumes the residual methane and decreases the hydrogen concentration. In addition, both of the reactions are very endothermic and require high temperatures and an atmospheric pressure, which result in successful conversions of methane. The evaluation of the CO_2/CH_4 ratio in a DRM reaction can be observed

showing the values of the CH_4 equilibrium conversion which are relative to the various temperatures shown in Figure 1[24].
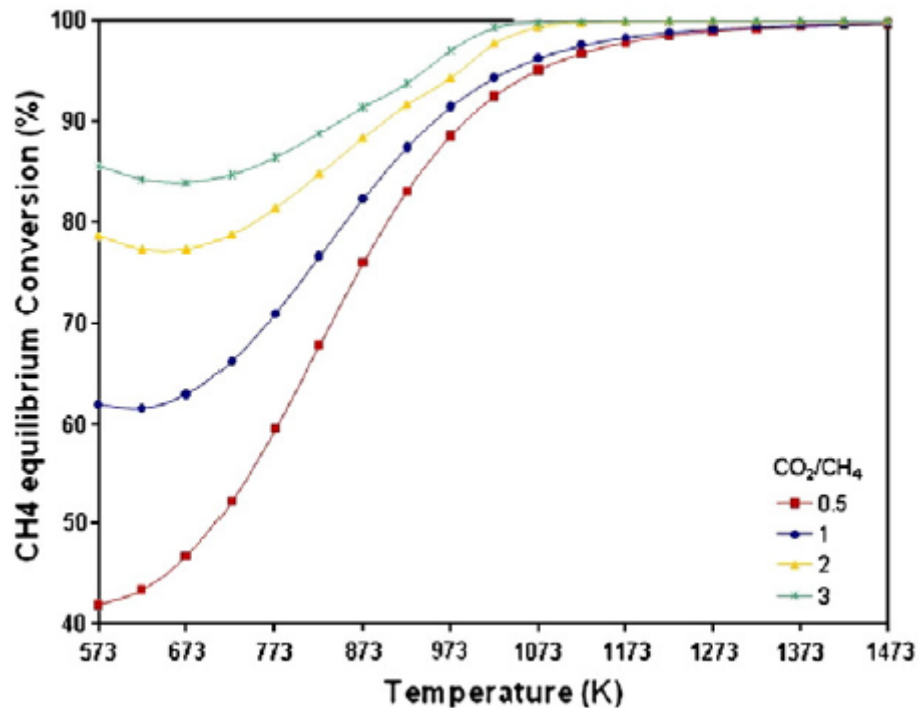
Figure 1 CH_4 equilibrium conversion various temperatures of CO_2/CH_4 ratio

Thermodynamic studies show that DRM reactions do not occur spontaneously at temperatures below 640 °C. Equation 2.1, shows a successful DRM reaction at temperatures > 723 °C[25]. Reverse water gas-shift (RWGS), as shown in equation 2.2, is greatly affected by the equilibrium in the temperature range of 650-850 °C. In this case, the DRM reactions are accompanied by the reaction of RWGS simultaneously. Equations 2.3-2.5 occur at temperatures > 850 °C. The hydrogenation of CO_2 and CO (equation 2.6-2.7) are much more favorable towards a RWGS reaction, especially at temperatures > 750°C and increase as does the temperature up to and including 1,000 °C. Another side reaction, CH_4 decomposition, shown in equation 2.8, is the carbon formation at temperatures > 557 °C. This reaction will be influenced by equilibrium limitations at the higher temperatures. The DRM reaction is endothermic and accumulates carbon from the CH_4 decomposition side reaction. For this occurrence, the catalyst is used for lowering the activation energy and improving the performance of this reaction.

As first reported in publications in the 1990's, the noble metals catalysts were used for dry reforming of methane. They have been shown to exhibit high activity in

methane and less sensitive to coking[x]. However, from an economic perspective, the noble metals aren't suitable for industrial level usage due to their high cost and restricted availability. The next step was the usage of a transition metal, such as Co, Mn, Fe and others which were widely used due to the noble metal economic factors. The nickel based catalyst is the most effective metal due to its high activity in methane, low cost and is easily obtainable. However, the major problem in this reaction is the accumulation of carbon on the surface of the catalyst. The morphology of the carbon formation on Ni is unique, with carbon forming whiskers beginning at the Ni-support interface and growing outward. Moreover, the support has the effect of this reaction due to its interaction with metal. This catalyst was used with various oxides support such as Al_2O_3, La_2O_3, CeO_2 , MgO, SiO_2, perovskite oxides, spinel[26-29].

2.2 Perovskite structure

The Russian mineralogist, Count Lev Aleksevich von Perovski, discovered the mineral perovskite ($CaTiO_3$) in the Ural Mountains in 1839 [30]. Much later, the first catalytic studies on perovskite catalysts were published in the beginning of the 1970s, reporting exceptional catalytic properties in oxidation reactions and NO reduction, when these catalysts were used instead the platinum-group metals in automotive exhaust catalytic convertors. Today, perovskites attract interest because their ease of preparation and low cost compared to noble metals and the advantage of this structure to accommodate a wide range of substituting and doping elements, allowing the tailoring of their properties to better target their applications [31].

Perovskite-type oxides are general formula ABO_3. the A cation is divalent and the B cation is tetravalent. At A cation there are lanthanides, such as Ce and La. At B cation there are thransition metal, such as Ni, Co, Mn and Fe. The ions occupying the A and B lattice sites are detailed in Figure 2.
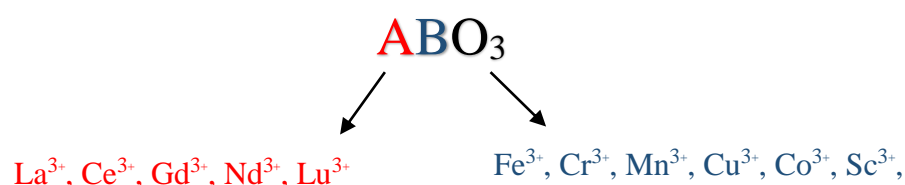
$$ABO_3$$

La^{3+}, Ce^{3+}, Gd^{3+}, Nd^{3+}, Lu^{3+} Fe^{3+}, Cr^{3+}, Mn^{3+}, Cu^{3+}, Co^{3+}, Sc^{3+},

Figure 2 Schematic of perovskite compositions

2.3 Literature review of perovskite catalyst for DRM reaction

Furthermore, numerous researches have been published regarding perovskite materials developed for high activity and stable catalysts for the dry reforming of methane. Several factors, such as conditions for the catalyst preparation, the preparation method, the basic supports and the addition of the promoter by partial substitution at site A and B were observed to improve the activity of catalysts and inhibit deactivation. Literature reviews of perovskite catalyst for DRM reaction are divided into four parts.

2.3.1 Preparation technique

The catalyst preparation methods have strong influence over physic chemical properties and performance of catalyst. Rivas et al.[32] prepared the $LaNiO_3$ perovskites by co-precipitation, sol-gel, and wet impregnation. All samples were calcined at 750 °C for 5 h. After the reduction step (10% H_2/N_2 at 700 °C for 2 h), the metallic nickel particle size depended on the preparation method. The co-precipitiation method shows the nickel dispersion lower than the impregnation method. The perovskite, prepared by coprecipitation after DRM reaction at 400 and 650 °C for 24 h, shows the highest CH_4 and CO_2 conversion and H_2/CO molar ratio. The XRD pattern of spent of the catalyst shows the hexagonal lanthanum oxycarbonate phase $La_2O_2CO_3$ and nickel metal. The CH_4 and CO_2 conversion of $LaNiO_3$ perovskite without reduction didn't show differences with the reduced sample. Chawla et al.[33] studied the preparation method of $LaNiO_3$ and $LaCoO_3$ perovskites catalyst by sol gel (SG), co-precipitation (CP) and impregnation (IM) method of DRM compared with the Ni/Al_2O_3(IM). The Ni/Al_2O_3 catalyst was loaded with different types of promoters to improve activity, selectivity and stability during long-term reaction. The $LaNiO_3$ (CP) perovskite showed the highest CH_4 and CO_2 conversion.

Valderrama et al.[7] investigated the use of perovskite-type solid solutions $La_{1-x}Sr_xCoO_3$ as precursors of highly dispersed Co nanoparticles to avoid coke formation during the dry reforming of methane under continuous flow of reactive gases. There catalysts were prepared by the auto combustion method and used as precursors for the catalytic methane dry reforming at 800 °C, atmospheric pressure under continuous flow of feed gases with a CH_4: CO_2 1:1 ratio. Catalysts formation of $LaSrCoO_3$ solid solutions was confirmed by the more intense diffraction peaks. It was observed that the activation/reduction process occurred through intermediary species producing Co^0 nano-size particles over the SrO and La_2O_3 phases, which were highly

dispersed in the $La_2O_2CO_3$-SrO solid matrix responsible for the high activity and low carbon formation after test catalytic. The display of Sr in doping quantities slightly promotes secondary reactions such as carbon formation and water gas shift retarding partially in this reaction.

In the recent past, Chiarello et al.[34] set up a flame-pyrolysis (FP) equipment for the one-step synthesis of perovskite mixed oxides $LaCoO_3$ perovskite and 0.5 wt% $Pd/LaCoO_3$ similar to that used for the preparation of different materials[35, 36]. The XRD pattern of $Pd/LaCoO_3$ during calcination in 21% O_2/He at the indicated temperatures is also shown in Figure 3. At 600 ºC, the surface area decreased to 20 m^2/g. After calcination at 800 ºC, the reflections of the perovskite became narrower and more intense, and the surface area decreased to 8 m^2/g. Calcination at 800 ºC caused sintering and substantial incorporation of Pd at the B-site of the ABO_3. Thermal resistance showed directly related to flame temperature, i. e. to the combustion enthalpy of the solvent, but a relatively high amount of residual organic matter can negatively affect this property.
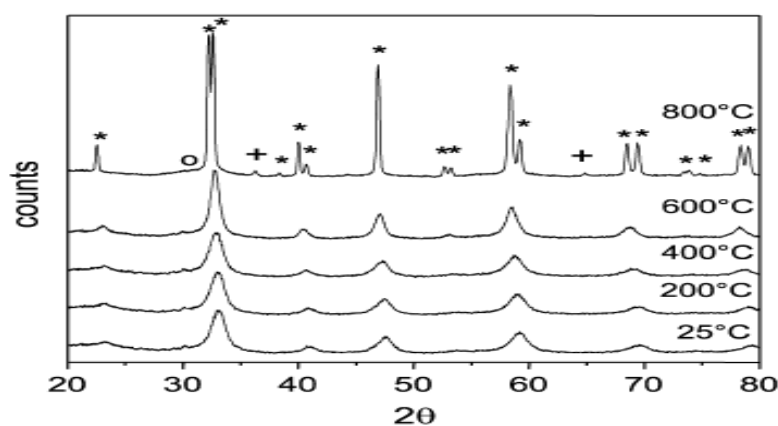
Figure 3 XRD of $Pd/LaCoO_3$ during calcination in 21%O_2/He at the indicated
temperatures: (□) $LaCoO_3$; (+) Co_3O_4; (o) La_2CoO_4 phases

2.3.2 Choice of support

Perovskite material was also used as a catalyst support for the DRM reaction. Barros et al.[37] reported the nickel catalyst prepared by impregnation method using the $BaTiO_3$ as support for the DRM reaction. All catalysts were tested at 800 ºC. The $Ni/BaTiO_3$ shows a higher CH_4 and CO_2 conversion than Ni/γ-Al_2O_3 catalyst. After the reduction step, the γ-Al_2O_3 showed a phase transition, but the $Ni/BaTiO_3$ remained unaltered. However, the γ-Al_2O_3 wxhibites higher acidity than the $BaTiO_3$

and catalyst didn't promote a favorite of CO_2 absorption. Therefore, its activity was lower than $BaTiO_3$

Wang et al. [38] developed the $LaNiO_3$ perovskite catalysts supported by mesoporous SBA-15, MCM-41 and Silica carrier for Dry Reforming of Methane. The catalysts were prepared via filling the pores of mesoporous silica with citrate complex precursors of nickel and lanthanum. The $LaNiO_3$/MCM-41 showed the highest initial catalytic activity due to the high Ni dispersion. The $LaNiO_3$/SBA-15 was more stable than the $LaNiO_3$/MCM-41 in the long-term reaction. Inaddition, the stable silica matrix was inhibited by the agglomeration of nickel species. The carbon deposition shows a dramatic decrease of the catalytic activity for $LaNiO_3$/SiO_2 catalysts.

The $LaNiO_3$/SBA 15 was modified in the perovskite by the second cation in the A and/or B site. The incorporation of the oxides into the perovskite generated a higher metal-support interaction, increasing the Ni reduction temperature. The CH_4 and CO_2 conversions that form the dry reforming of methane reaction at 600 °C and 700 °C for 24 h are shown in table 1. The CH_4 and CO_2 conversion decrease when added to the A or B of the bulk perovskite as reported by Rivas et al.[13].

Table 1 Catalytic results of perovskite oxides bulk and built-in a SBA-15.

Catalyst precursor	X_{CH4} (%)	X_{CO2} (%)	H_2/CO (molar ratios)
$LaNiO_3$[a]	85	87	0.90
$La_{0.8}Ca_{0.2}NiO_3$[a]	55	71	0.80
$La_{0.8}Ca_{0.2}Ni_{0.6}Co_{0.4}O_3$[a]	66	80	0.80
$LaNiO_3$/SBA-15[a]	88	91	0.90
$La_{0.8}Ca_{0.2}NiO_3$/SBA-15[a]	82	88	1.00
$La_{0.8}Ca_{0.2}Ni_{0.6}Co_{0.4}O_3$/SBA-15[a]	86	88	1.00
$LaNiO_3$/SBA-15[b]	63	74	0.87
$La_{0.8}Ca_{0.2}NiO_3$/SBA-15[b]	69	70	1.04
$La_{0.8}Ca_{0.2}Ni_{0.6}Co_{0.4}O_3$/SBA-15[b]	53	65	0.84

a Treaction = 700 °C

b Treaction = 600 °C; CH_4:CO_2:Ar = 1:1:8; VE = 24 $L^{-1}g^{-1}$; m_{cat} = 200 mg; P = 1 atm; time = 24 h

2.3.3 Addition of promoter by partial substitution at site A

The important advantage of using perovskite-type structures is the possibility of total or partial substitution of A and B cations, which modify the redox properties of the catalyst and catalytic activity. Bhavani et al.[39] investigated barium substituted lanthanum manganite $La_{1-x}Ba_xMnO_3$ (x = 0.10-0.50) perovskite for dry reforming of methane. The Ba/Mn ratio of 0.10 and 0.15 showed a high surface area with uniform particle and pores. The catalytic activity shown in Figure 4. The $La_{0.85}Ba_{0.15}MnO_3$ showed a high CH_4 and CO_2 conversions, a H_2/CO ratio and a minute coke formation. It was better than more other Ni based catalysts of lanthanum manganite.
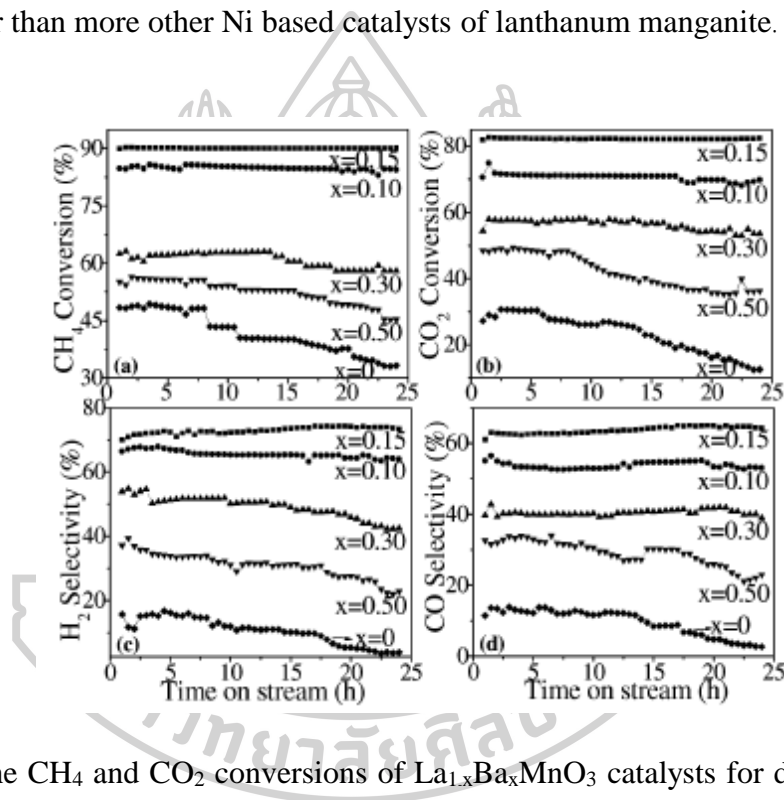
Figure 4 The CH_4 and CO_2 conversions of $La_{1-x}Ba_xMnO_3$ catalysts for dry reforming of methane; a) CH_4 conversion, b) CO_2 conversion, c) H_2 selectivity and d) CO selectivity.

Mixed oxides $La_{1-x}Ce_xNiO_3$ (x = 0, 0.05, 0.4 and 0.7) was prepared by the citrate method and tested in the CH_4 dry reforming of methane with CO_2 reaction. The $LaNiO_3$ perovskite shows higher activity in CH_4 conversion, it undergoes a slow deactivation with time on stream. Yet, the substitution of the A site metal ion with Ce led to an increase in the CH_4 and CO_2 conversions and increased the stability of the catalysts with respect to the reforming reaction. These results were reported by Lima et al.[40].

Yang et al.[41] developed that $La_{0.9}M_{0.1}Ni_{0.5}Fe_{0.5}O_3$ (M = Sr and Ca) for CH_4 dry reforming with CO_2. Diffraction patterns of prepared $LaNi_{0.5}Fe_{0.5}O_3$ and $La_{0.9}M_{0.1}Ni_{0.5}Fe_{0.5}O_3$ (M = Sr and Ca) were presented in Figure 5. Since the substitution amount of the promoter metals (Ca/Sr) was very small, few changes in XRD patterns were observed. The effect of partial substitution of La with Sr/Ca was investigated in the dry reforming reaction of methane for H_2/CO ratio. The XRD patterns change slightly when the partial substitution of a small amount of the promoter metals (Ca/Sr). The $La_{0.9}Ca_{0.1}Ni_{0.5}Fe_{0.5}O_3$ catalyst exhibit the highest catalytic activity and resistances to carbon during the long-time reaction.
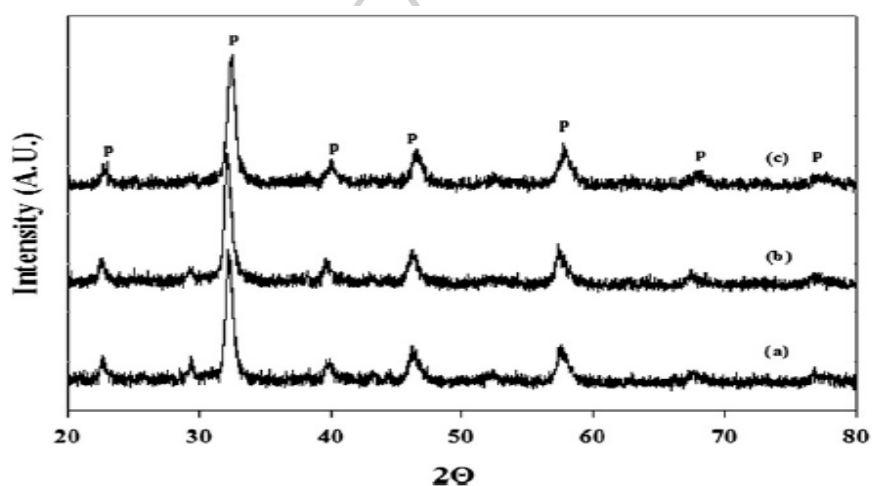
Figure 5 XRD patterns of prepared catalysts before the reaction: (a) $LaNi_{0.5}Fe_{0.5}O_3$,

(b) $La_{0.9}Sr_{0.1}Ni_{0.5}Fe_{0.5}O_3$, (c) $La_{0.9}Ca_{0.1}Ni_{0.5}Fe_{0.5}O_3$. (P perovskite).

2.3.4 Addition of promoter by partial substitution at site B

The Co substituted nickel perovskite was also used for dry reforming of methane, focusing at better dispersing of the active nickel species at the surface of the support. Sierra et al.[42] obtained cobalt substituted lanthanum nickelate ($LaNiO_3$) in methane dry reforming. The evolution of CH_4 and CO_2 conversions were shown in Figure 6. The presence of cobalt showed a decrease of CH_4 and CO_2 activity due to Co-Ni alloy formation. Nevertheless, the stability of the carbon deposition was increased in the cobalt.
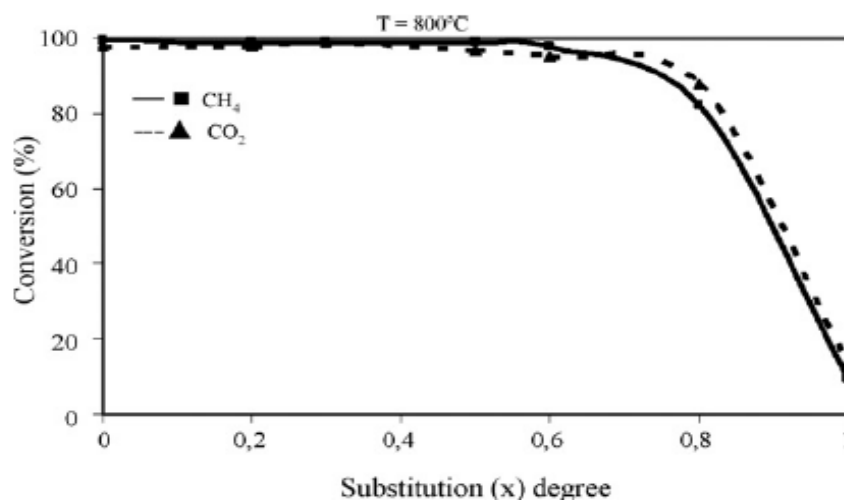
Figure 6 CH_4 and CO_2 conversions on unreduced $LaNi_{1-x}Co_xO_3$ at 800 °C.

Provendier et al.[43] studied the iron in $LaFe_{1-x}Ni_xO_3$ for DRM at 800 °C for 25 h. The addition of iron did not affect the catalytic activity, but strongly (increased) stability. It did not (create or affect) the carbon deposition during the reaction. Moradi et al.[44] showed good activity and stability of $LaNi_{0.8}Zn_{0.2}O_3$ perovskite for CO_2 reforming of CH_4. TPR results showed that partial substitution of Ni by Zn increased the temperatures of reduction peaks, leading to the more stable perovskite structure compared to $LaNiO_3$ structure. It indicated that Zn stabilizes the perovskite structure. In addition, TGA (Figure 7) results showed that $LaNi_{0.8}Zn_{0.2}O_3$ was more resistant to coke formation in comparison with $LaNiO_3$ during 75 h time on stream stability test.

Figure 7 TGA oxidation curves of the used $LaNi_{0.8}Zn_{0.2}O_3$ and $LaNiO_3$ after 75 h of reaction.

CHAPTER III

EXRERIMENTAL

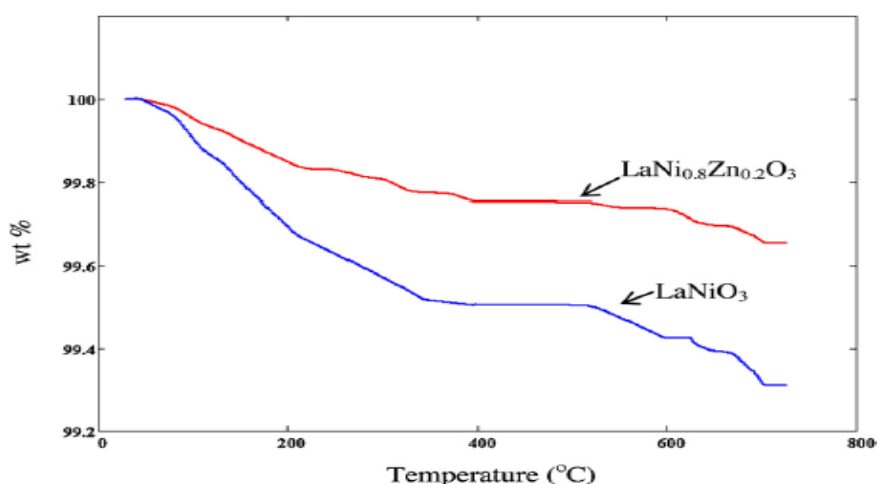This part is divided into three parts consisting of catalyst preparation, catalyst characterization and the catalytic activity test. The first part explains catalyst preparation by flame spray pyrolysis (FSP) and incipient wetness impregnation methods. The second part explains catalyst characterization using different techniques containing X-ray diffraction (XRD) , N_2 physisorption, temperature programmed reduction (TPR) , Thermogravimetric analysis (TGA) and X-ray photoelectron spectroscopy (XPS) and the X-ray absorption (XAS) , which these techniques were using for catalyst part 2. Finally, a detailed procedure for catalyst evaluation in the carbon dioxide reforming of methane is explained.

3.1 Catalyst preparation

The catalysts were prepared by two methods. The $LaCoO_3$ perovskites were prepared by flame spray pyrolysis (FSP) and Ni was loaded by the incipient wetness impregnation method. The chemicals used in this research are shown in table 2.

Table 2 The details of chemicals used in the catalyst preparation

Chemicals	Formula	Grade (%)	Manufacture
Lanthanum (III) nitrate hexahydrate	$LaN_3O_9 \cdot 6H_2O$	99	Sigma-Aldrich Cheme GmbH, Germany
Cobalt (II) nitrate hexahydrate	$Co(NO_3)_2 6H_2O$	98	Ajax Finechem.Pty Ltd
Cerium(III) nitrate hexahydrate	$Ce(NO_3)_3 \cdot 6H_2O$	99	Sigma-Aldrich Cheme GmbH, Germany
Manganese (II) nitrate tetrahydrate	$Mn(NO_3)_2 4H_2O$	99	Ajax Finechem.Pty Ltd

Chemicals	Formula	Grade (%)	Manufacture
Copper(II) nitrate trihydrate	$Cu(NO_3)_2 \cdot 3H_2O$	98	Sigma-Aldrich Cheme GmbH, Germany
Zinc (II) nitrate hexahydrate	$Zn(NO_3)_2 \cdot 6H_2O$	98	Ajax Finechem.Pty Ltd
Ethanol	C_2H_5OH	98	J.T.Baker

The FSP reactor is used for preparation of catalysis. Figure 8 shows scheme of flame spray. The $LaCoO_3$ perovskite-type oxides were prepared by flame spray pyrolysis. The cobalt (II) nitrate hexahydrate ($Co(NO_3)_2 \cdot 6H_2O$) and lanthanum (III) nitrate hexahydrate ($LaN_3O_9 \cdot 6H_2O$) were diluted with an ethanol solution to 0.5 M. After that, the solution was transferred to an ultrasonic bath for 30 min and stirred. Using a specifically designed enclosed chamber the mixed liquid precursor was projected towards a CH_4/O_2 flame using a syringe pump and dispersed by O_2. The fine spray was created by the use of a capillary tip and evaporated into the flame. The $LaCoO_3$ material was collected on a glass microfiber filter utilizing a vacuum pump. These FSP-made $LaCoO_3$ oxides were divided into two parts. One was calcined in airflow at 800 °C for 4 h and denoted as LC. Another was the starting material for the catalyst preparation.
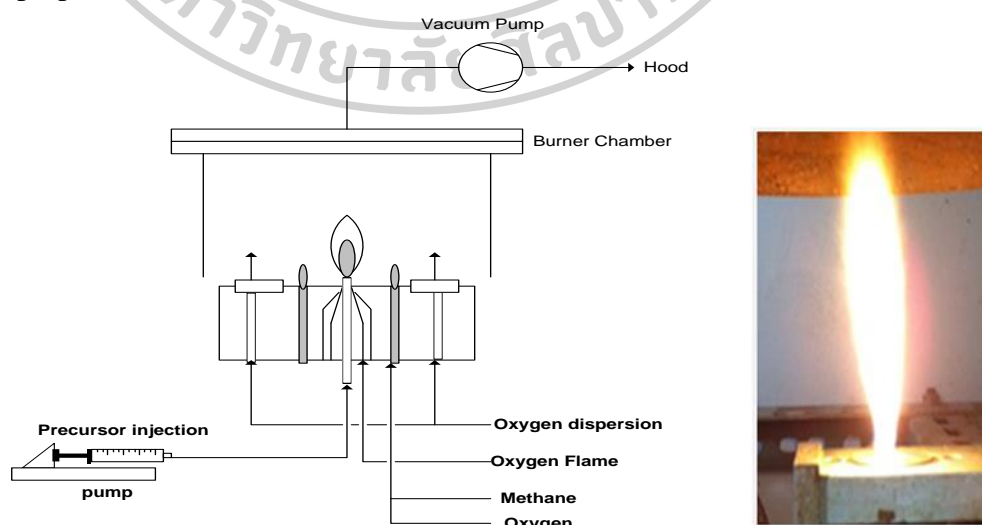

Figure 8 Experimental set-up scheme of flame spray pyrolysis

The preparation is divided into three parts. First, the Ni metal solution (nickel nitrate) was impregnated into the FSP-made $LaCoO_3$ support. The nickel loading is varied at 0, 2, 5 and 10 wt%. After the incipient wetness impregnation, the material was dried at 110 °C for 12 h and then calcined in airflow at 800 °C for 4 h. The catalyst and catalyst symbols are shown in Figure 9 and 10. The appropriate nickel loading is selected. It was used in part 2 and 3.

Catalysts (LC from LaCoO₃ perovskite)
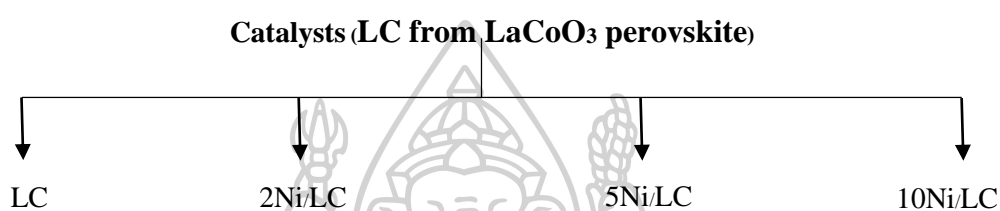

| LC | 2Ni/LC | 5Ni/LC | 10Ni/LC |

Figure 9 The catalyst symbol of $LaCoO_3$ catalyst with varying Ni

Figure 10 The catalysts were prepared by FSP synthesis

Next part, the $Ce_xLa_{1-x}CoO_3$ (x = 0.0, 0.2, 0.4, 0.6, 0.8 and 1.0). catalysts were prepared by flame spray pyrolysis (FSP), Using the same condition as part 1. The catalyst symbols are shown in table 3.

Table 3 The catalyst symbol of $Ni/Ce_xLa_{1-x}CoO_3$ catalyst with varying Ce/La ratio

Catalyst
x = 0.0
x = 0.2
x = 0.4
x = 0.6
x = 0.8
x = 1.0

Finally, the Co position was substituted by the transition metal (Mn, Zn and Cu). The catalysts were prepared by flame spray pyrolysis (FSP). And then, the transition metals were selected and it partially substituted each into the Co position which resulted in $Ni/LaB_yCo_{1-y}O_3$(y = 0, 0.05, 0.1, 0.5, and 1.0). The detail is shown in Figure 11.
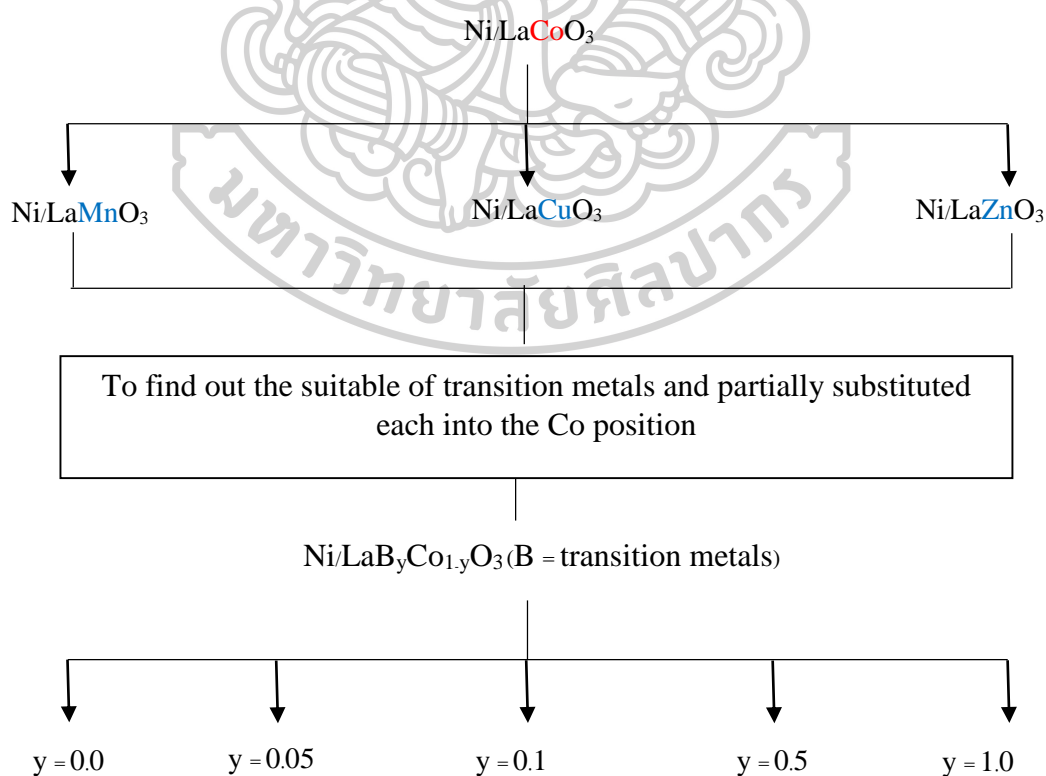
Figure 11 The catalyst symbol of catalyst

3.2 Catalyst characterization

3.2.1 X-ray diffraction (XRD)

The bulk crystal structure, crystalline size, and chemical phase composition were analyzed using X-ray diffractometer SIEMENS D-5000 diffractometer with a Cu Kα radiation source. The XRD patterns were recorded in the range 2θ from 20 to 80º. The crystallite sizes are assessed from line broadening according to the Scherrer equation and α-Al$_2$O$_3$ is used as standard.

3.2.2 N$_2$ physisorption

The surface area and pore characteristics were determined using BET BELSORP MINI Π JAPAN. The samples were degasified in He gas flow of 50 ml/min at 150 ºC for 3 h. The catalyst cell was dipped in the dewar containing liquid nitrogen. The N$_2$ adsorption-desorption was measured by the different partial pressure of N$_2$ at -196 °C.

3.2.3 Temperature programmed reduction (TPR)

Temperature programmed reduction (TPR) experiments were performed using a Micromeritics AutoChem 2910. A 0.1 g of a catalyst sample is placed in a quartz tubular reactor. Under nitrogen atmosphere at a flow rate of 30 ml/min, the catalyst sample is heated up to 150 ºC at a heating rate of 10 ºC/min. The catalyst samples in a quartz tubular reactor was reduced from 100 ºC to 800 ºC at a heating rate of 10 ºC/min in 10% H$_2$/N$_2$ flow gas of 30 ml/min. During the reduction step, the water produced in the process was trapped by the liquid nitrogen.

3.2.4 Thermogravimetric analysis (TGA)

Thermogravimetric analysis (TGA) was performed by SDT Q600 equipment. The sample was heated from room temperature up to 1000 °C in a heating rate of 10ºC/min under a flow of air atmosphere to measure loss of the catalyst weight.

3.2.5 X-ray photoelectron spectroscopy (XPS)

The lanthanum oxide and cerium oxide of the catalysts were analyzed by X-ray photoelectron spectroscopy (XPS) at the SLRI-XPS beamline (BL5.3) at the Synchrotron Research Institute (Public Organization), Nakhon Ratchasima, Thailand.

3.2.6 X-ray absorption (XAS)

The X-ray absorption (XAS) near edge spectra (XANES) of Ce and La were collected in transmission mode at the SLRI-XAS beamline (BL8) at the Synchrotron Research Institute (Public Organization), Nakhon Ratchasima, Thailand.

3.3 The catalytic activity test

The DRM was tested in a quartz tubular reactor under atmospheric pressure. A catalyst sample is packed in a quartz tubular reactor with placed in the furnace. Prior to the catalytic activity test, the catalyst sample was heated up to 500 °C in argon flow rate of 60 ml/min with a heating rate of 10 °C/min and the catalyst is reduced by hydrogen with flow rate of 60 ml/min at 500 °C for 2 h. After the reduction, the temperature was increased to 700 °C by argon flow and the CH_4 and CO_2 with the molar ratio of CH_4/CO_2 as 1 was introduced. The total volumetric flow rate was 40 ml/min to maintain GHSV wequal to 12,000 h^{-1}. The products of the reaction were collected hourly for 15 h. The composition of the product stream was analyzed on-line by gas chromatograph connecting with Porapak Q column and thermal conductivity detector (TCD). Schematic diagram of the reaction line shown in Figure 12.
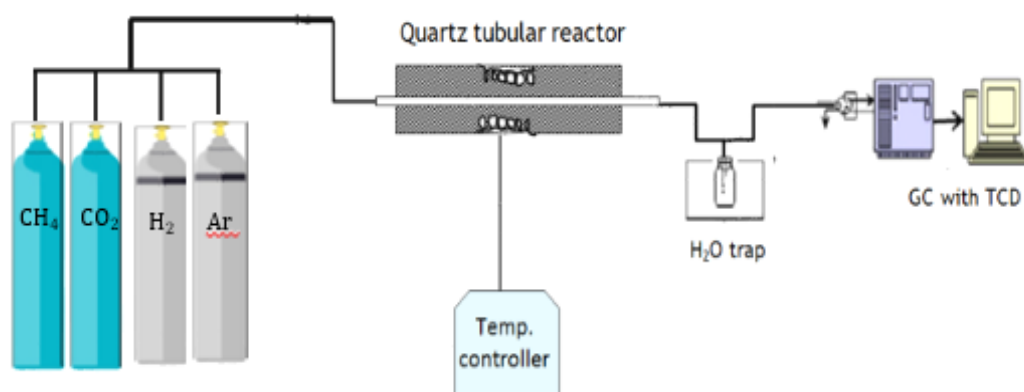

Figure 12 Scheme of CO_2 reforming of CH_4 reaction line

CHAPTER IV
RESULTS AND DISCUSSION

The results and discussion in this chapter are divided into three parts; the effect of Ni loading, the Ce partial substitution into La position and the transition metals (Cu, Mn and Zn) substitution into Co position. These are the results of physical and chemical properties of nickel based catalysts and the catalytic activity tests.

First, the $LaCoO_3$ perovskites were prepared by flame spray pyrolysis (FSP), it was studied effect of the temperatures during calcination. The $LaCoO_3$ was prepared by FSP method and show no calcination as shown $LaCoO_3$ symbol. The second sample was also prepared by FSP method and calcined at 500°C as shown $LaCoO_3$ 500°C symbol. The third samples were also prepared by FSP method and calcined at 800 °C as shown $LaCoO_3$ 800 °C. The X-ray diffraction spectra of samples with different temperatures during calcination are shown in Figure 13. The $LaCoO_3$ shows low crystallinity and the surface area was 27.4 m²/g. The $LaCoO_3$ 500 °C showed an increase in the intensity of the $LaCoO_3$ peaks, but the surface areas decreased 15.2 m²/g due to the metal sintering[11]. The $LaCoO_3$ 800 °C showed high, narrow and intense peaks, but the surface areas decrease to 6.1 m²/g. However, the perovskite catalysts are the crystallize oxide. The temperatures calcination at 800 °C was used for three part.
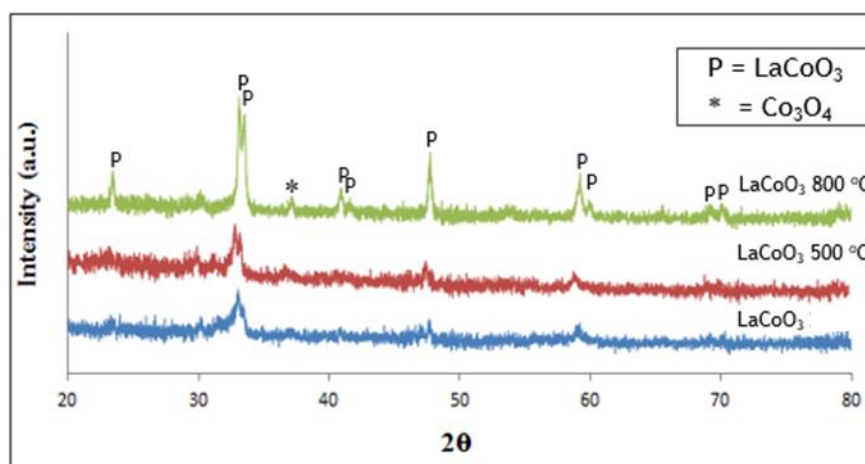

Figure 13 XRD patterns of $LaCoO_3$ with different temperatures during calcination

4.1   The effect of Ni loading on LaCoO₃ perovskites

The physical and chemical properties of the catalysts were focused on. The phase identification and the average crystalline size were determined using the X-ray diffraction technique. The BET surface area, the pore characteristics and the average particle size were determined by the nitrogen physisorption. The temperature programmed reduction (TPR) exhibited reduction behavior and reducibility of the catalysts. The weight loss and derivative weight loss of all spent catalysts were obtained after the DRM reaction was investigated by using TG.

The X-ray diffraction spectra of samples with different Ni loading are shown in Figure 14. All of the XRD patterns of the fresh catalysts show only LaCoO₃ crystalline phase as seen in Figure 14a. This phase was in agreement with the literature [45, 46]. These results showed that the preparation by FSP in the single step can generate the LaCoO₃ phase with a high purity crystallinity. The calcination after adding Ni can maintain the perovskite structure but decrease the degree of its crystallinity. Figure 14b shows the XRD pattern of the catalysts after reduction. For all catalysts, the XRD peaks of LaCoO₃ phase disappeared but the La₂O₃ phase were found. The CoO peak was clearly observed for only LC catalyst. This indicated that during the reduction step the LaCoO₃ perovskite structure was destroyed, which resulted in the cobalt species dispersed on the La₂O₃ phase[47]. The 2Ni/LC and 5Ni/LC showed high crystallinity of La₂O₃ compared to the LC. On the other hand, the intensity of La₂O₃ peaks in the 10Ni/LC was very low because the catalyst surface was covered by much more nickel species[48].
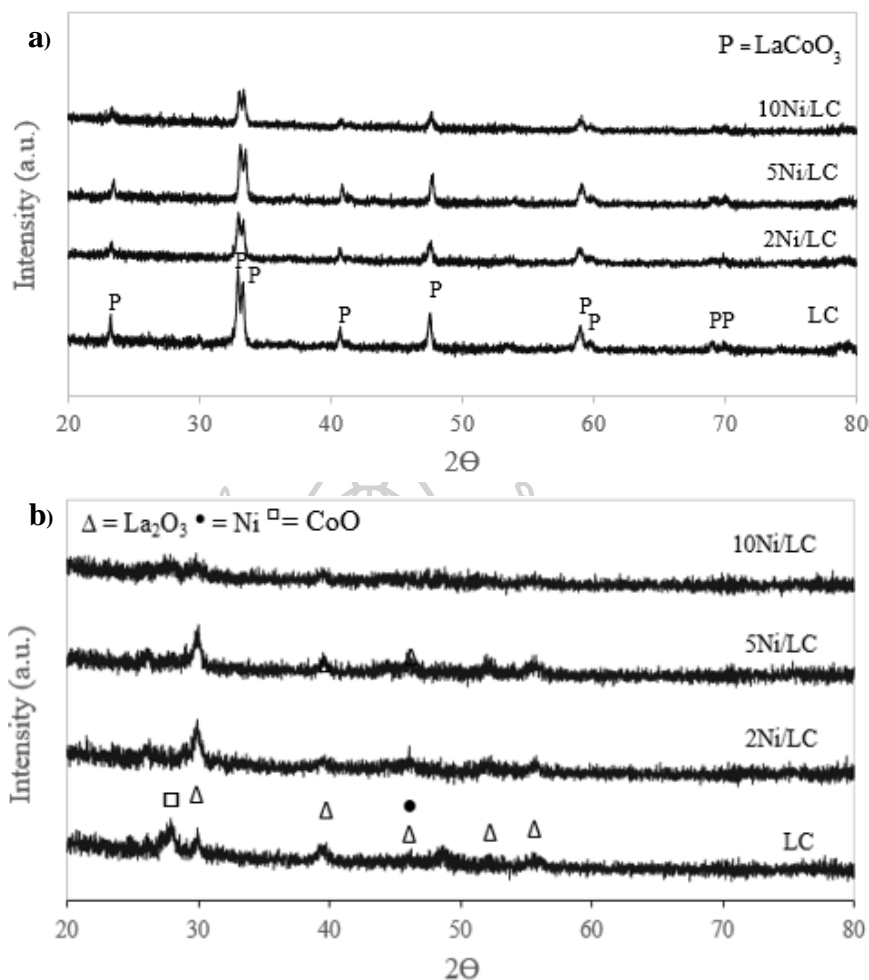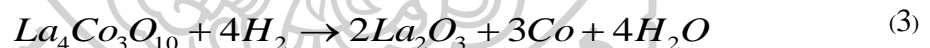
Figure 14 a)XRD patterns of samples xNi/LC (x = 2-10 wt.%),b) samples after reduction
at 500 $^{\circ}$C and c) after test catalytic at 700 $^{\circ}$C

The BET surface area and the average pore diameter obtained by N_2
physisorption are shown in table 4. The data of N_2 physisorption for the uncalcined
$LaCoO_3$ oxides were also collected but not shown here. It was found that after
calcination the BET surface area of the $LaCoO_3$ support was significantly decreased
from 27.4 to 6.1 m^2/g. This result indicated the metal sintering occurred by the
calcination at high temperature [11]. The surface area decreases when the Ni loading is
increased with the exception of 5Ni/LC due to LC was impregnated with Ni before
calcination occurs at a temperature of 800 $^{\circ}$C [49].

Table 4 The BET surface area (S_BET), the average pore diameter (D_pore), XRD data of Ni based

Catalyst	S_{BET} (m²/g)	D_{pore} (nm)	XRD initial phase	XRD after reduction (500 °C)	XRD after reaction (700 °C)
LC	6.1	7.3	$LaCoO_3$	CoO, La_2O_3	$La_2O_2CO_3$
2Ni/LC	3.4	6.1	$LaCoO_3$	La_2O_3	$La_2O_2CO_3$
5Ni/LC	8.7	6.1	$LaCoO_3$	La_2O_3	$La_2O_2CO_3$
10Ni/LC	1.9	6.4	$LaCoO_3$	La_2O_3	$La_2O_2CO_3$

Figure 15 shows the reduction characteristics of all catalysts. For the LC, there were two main reduction regions a t below and above 400 °C. The first region was assigned as overlap of two reduction steps. The $LaCoO_3$ was first reduced to form $LaCoO_{2.75}$ and then $La_4Co_3O_{10}$ as shown in the equations (1) and (2). Valderrama et al. reported that the $LaCoO_3$ phase was destructed, which assured the mobility of oxide ions. The reduction of $La_4Co_3O_{10}$ to create La_2O_3 and Co metal was proceeded in the second region at high temperature as shown in the equation (3). This was implied to strong interaction of Co metal and La_2O_3 support [22]. In addition, a broad peak at 400-500 °C show the intermediate formation of La_2CoO_4 [14].

$$LaCoO_3 + 0.25H_2 \rightarrow LaCoO_{2.75} + 0.25H_2O \tag{1}$$

$$4LaCoO_{2.75} + H_2 \rightarrow La_4Co_3O_{10} + Co + H_2O \tag{2}$$

$$La_4Co_3O_{10} + 4H_2 \rightarrow 2La_2O_3 + 3Co + 4H_2O \tag{3}$$

The introduction of Ni showed that both regions were shifted to higher temperature and their positions were closer. The percentage of reduction can be observed in table 5, indicating the 2Ni/LC shows the highest reducibility. When increasing the Ni loading by 5 and 10 wt%, the results decrease the reducibility due to having large Ni metal and decrease the formation of perovskite structure.
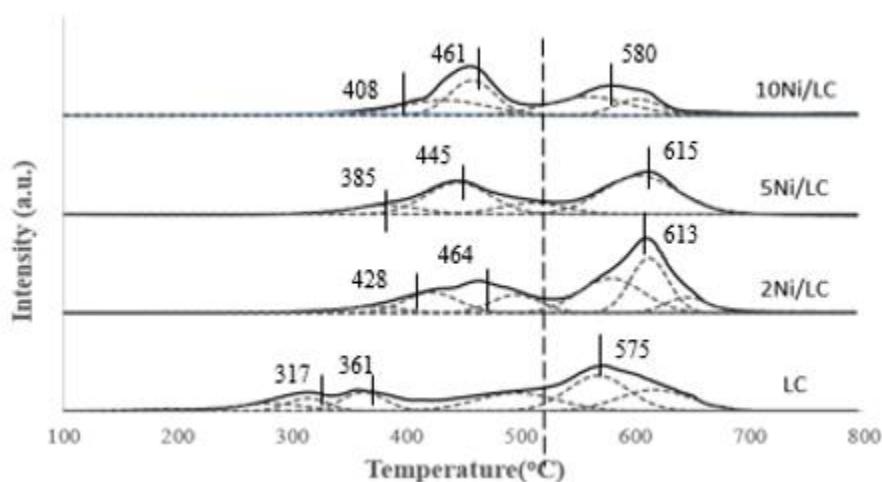
Figure 15 TPR profile of xNi/LC (x = 2-10 wt.%) catalysts

The CH_4 conversion of the xNi/LC catalysts for dry reforming of methane at 700 °C for 15 h were reported as shown in table 5. The LC catalyst was rather inactive for the DRM reaction. It was reminded that before the catalytic test the reduction of this catalyst was occurred at 500 °C. From the TPR profile (Figure 15), it was implied that at the reduction temperature of 500 °C the $LaCoO_3$ structure can be hardly reduced to produce the La_2O_3 structure, which was necessary for an initial activation of CO_2 to form $La_2O_2CO_3$ phase. When adding Ni in the perovskite support, the catalytic activity was very high. It was notable that conversion of CO_2 was higher than that of CH_4. The Ni sites was more active than the Co sites in this reaction and therefore the CH_4 was first adsorbed and activated on the surface of Ni metal. The Ni active sites were well known to promote the reverse water gas shift reaction (RWGS) [50]. This resulted in more production of CO. The 2Ni/LC catalyst showed the highest CH_4 and CO_2 conversions and H_2/CO ratio as shown in table 5. Additionally, the CH_4 conversion was decreased with increasing Ni loading but the CO_2 conversion was rather constant. A high amount of Ni promoted the reverse water gas shift reaction and therefore the difference in the CH_4 and CO_2 conversions referred to the Co and Ni activities over the La_2O_3 support.

Table 5 CH_4 and CO_2 conversion (%), H_2/CO ratios, weight loss determined in the TG oxidation tests and percentage of reduction of Ni based.

Catalyst	Initial (1h)			Final (15h)			Weight loss TG (%)	Reducibility (%)
	$X_{CH4\%}$	$X_{CO2\%}$	H_2/CO	$X_{CH4\%}$	$X_{CO2\%}$	H_2/CO		
2Ni/LC	31	64	0.57	66	77	0.86	23.2	86.7
5Ni/LC	34	67	0.61	58	79	0.74	36.7	67.0
10Ni/LC	13	57	0.43	39	71	0.63	49.5	42.3

Figure 16 shows the XRD signal of this spent catalyst. For all spent catalysts the $La_2O_2CO_3$ phase was formed due to the La_2O_3 reacting with the CO_2 reactant during the DRM [50]. The 2Ni/LC shows the highest intensity $La_2O_2CO_3$ phase, which played a very important role in this reaction. It can inhibit carbon formation and improve the catalytic activity and stability [12]. The 5Ni/LC and 10 Ni/LC, the results were identical and showed a $La_2O_2CO_3$ phase and a La_2O_3 phase. This was due to having large Ni metal which it has high of carbon formation with relative with TGA results [14].
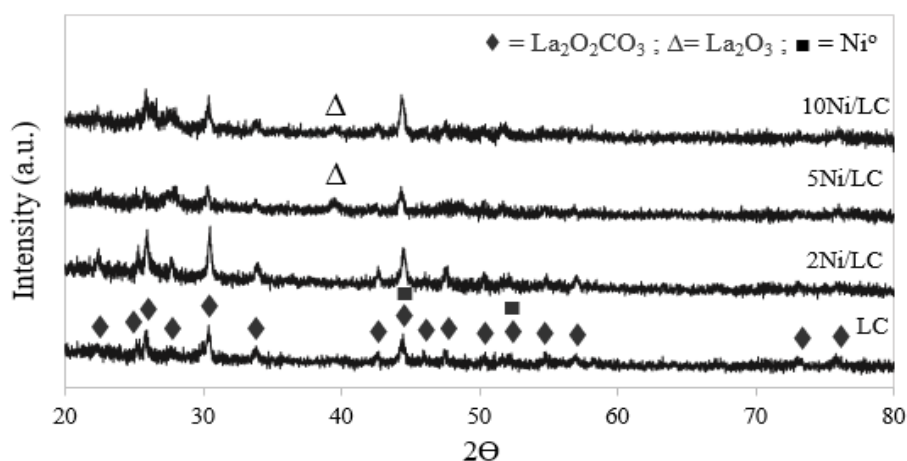

Figure 16 XRD patterns of samples after test catalytic at 700 ºC

The weight loss and derivative weight loss of all spent catalysts obtained after DRM reaction at 700 $^{\circ}$C for 15 h were investigated by using TGA as shown in Figure 17. The increase in LC catalyst weight in the temperature range of 380–820 °C was mainly due to the re-oxidation of metallic species [51]. This results can be calculated with TPR results. The elements in the catalyst can be found in table 6. When increase Ni loading, the La_2O_3 phase increased with the exception of 2Ni/LC due to the La_2O_3 can form together with Co to produce the highest amount of $LaCoO_3$ perovskite. All Ni based catalysts showed two regions of the weight loss (Figure 17). The first region occurred in the range of 300 and 550 °C. This weight loss has been attributed to the oxidation of the amorphous carbon, which is the active species in the formation of synthesis gas [40]. The second weight loss above 700 °C has been attributed to the decomposition of La carbonates [52]. The weight loss comparison can be seen in table 6. Since the 2Ni/LC catalyst resulted in only a 23.2 % weight loss, which causes less carbon formation, the $La_2O_2CO_3$ phase to be the preferred mechanism, confirming the XRD results. Subsequently, carbon is removed from the surface by the following reaction (Eq. (1)). The 5Ni/LC and 10 Ni/LC show higher weight loss, respectively due to high amorphous carbon.
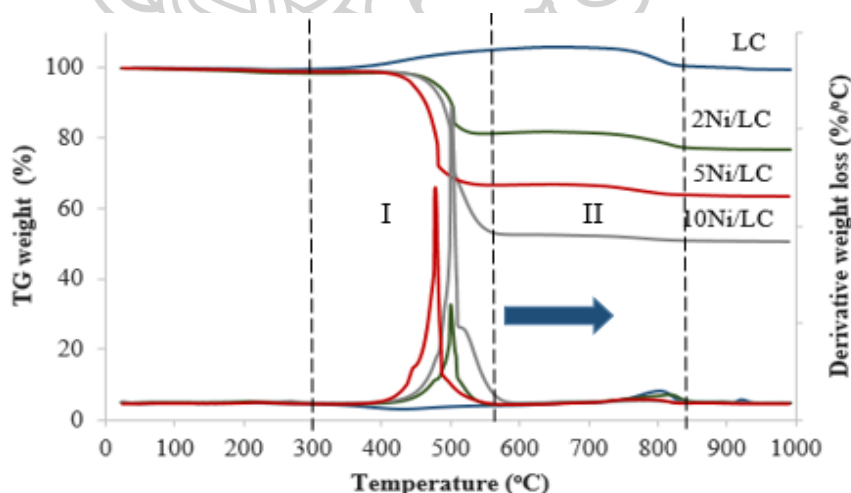
$$C - Ni + La_2O_2CO_3 \rightarrow 2CO + Ni + La_2O_3 \qquad (1)$$

Figure 17 TG and DTG profile of Ni/LC catalysts

Table 6 Formation of catalysts from TPR & TG

Catalyst	Co_3O_4 (%)	NiO (%)	La_2O_3 (%)	$LaCoO_3$ (%)
LC	8.4	-	9.7	81.9
2Ni/LC	5.1	1.5	6.7	86.7
5Ni/LC	12.3	6.5	14.2	67.0
10Ni/LC	18.8	17.1	21.8	42.3

4.2 Effect of the Ce partial substitution into La position

The physical and chemical properties of the catalysts were determined using different techniques containing X-ray diffraction (XRD) , N_2 physisorption, temperature programmed reduction (TPR), Thermogravimetric analysis (TGA), X-ray photoelectron spectroscopy (XPS) and the X-ray absorption (XAS).

Figure 18 shows an X-ray diffraction spectra of samples with different ratio Ce substitutions. The XRD peak at 23.1, 32.8, 40.6, 47.3, 58.4, 69.6 and 79.1 were assisgned to be the $LaCoO_3$ perovskites phase as seen in Figure 18a [53]. The inserting Ce at x=0.2 can maintain the perovskite structure but decreases the degree of its crystallinity. Besides, the inserting of more than x=0.2 showed evidence of only CeO_2 peaks (table 7). This is because the dilution of perovskite structure by the ceria support[54]. The very sharp peak of CeO_2 phases clearly showed an increased ratio of Ce/La. Figure 18b shows the XRD pattern of the catalysts after reduction. The XRD peaks of $LaCoO_3$ phase disappeared, but the La_2O_3 phase was found with only x=0. During the reduction step, the $LaCoO_3$ perovskite structure was destroyed. This resulted in the cobalt species being dispersed in the La_2O_3 phase[47]. When increasing the ratio of Ce/La, the catalysts of more than x=0 disappear in La_2O_3 phase. However, the CeO_2 phase was found with an increase of the degree of CeO_2 crystallinity. The data of the phase, which was obtained by XRD spectra, was included in table 7.
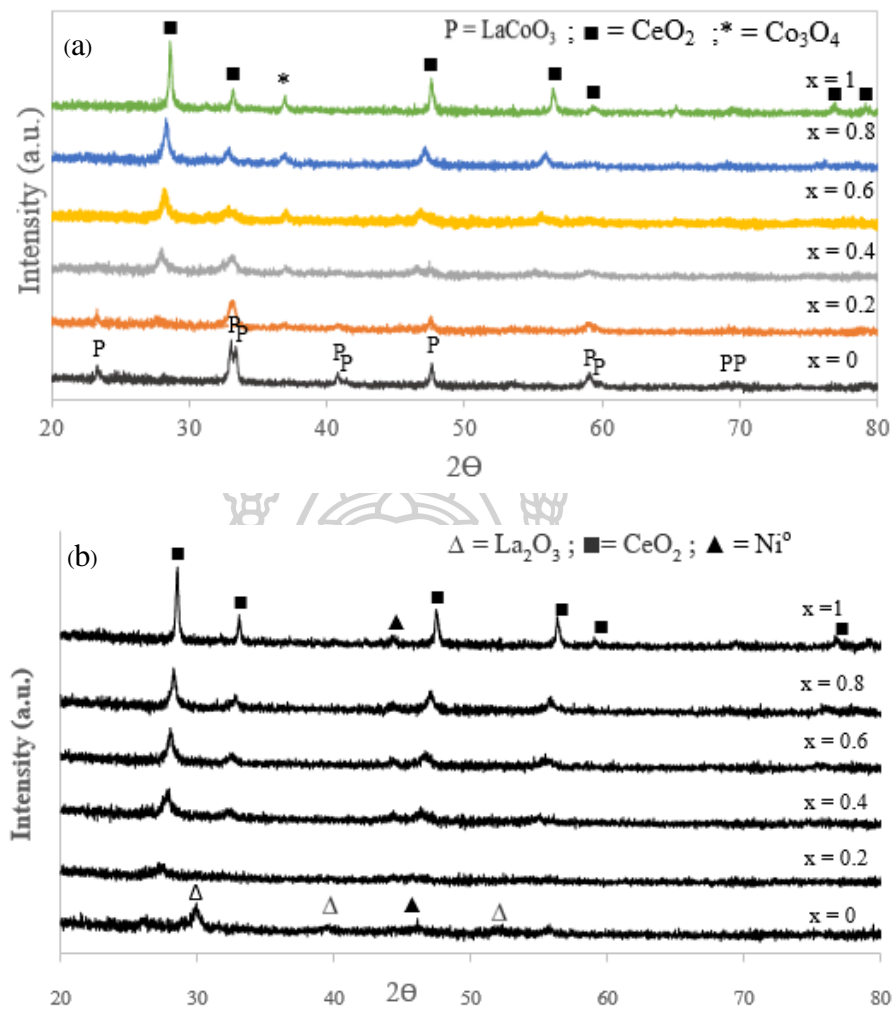
Figure 18 XRD patterns of samples 2Ni/LaC (x =2-10 wt%)(a), samples after reduction at 500 °C(b).

Table 7 The BET surface area (S_{BET}) and XRD result of $2Ni/Ce_xLa_{1-x}CoO_3$

Catalyst	S_{BET} (m²/g)	Crystalline size (nm) Initial phase CeO₂	XRD initial phase	XRD after reduction (500 °C)	XRD after reaction (700 °C)
x = 0.0	3.4	-	$LaCoO_3$	La_2O_3	Ni, $La_2O_2CO_3$
x = 0.2	6.3	-	$LaCoO_3$	CeO_2	Ni, $La_2O_2CO_3$
x = 0.4	8.4	6.6	$LaCoO_3, CeO_2$	CeO_2	CeO_2
x = 0.6	8.1	20.3	CeO_2	CeO_2	CeO_2
x = 0.8	11.5	30.8	CeO_2	CeO_2	CeO_2
x = 1.0	7.1	49.0	CeO_2	CeO_2	CeO_2

The BET surface area (S_{BET}) obtained by N_2 physisorption are shown in table 7. When increase inserting Ce were significantly increased from 3.4 to 11.5 m²/g. The surface area increases when the Ce inserting due to the Ce effect was supplemented with cobalt. The surface area at x= 1.0 shows 7.1 m²/g. The adsorption-desorption isotherms of all catalyst displayed IV type and a hysteresis loop of the H_2 hysteresis according to IUPAC classification as shown in Figure 19. This isotherm is mesoporous pores with tubular-shaped capillaries opening at both ends[55].
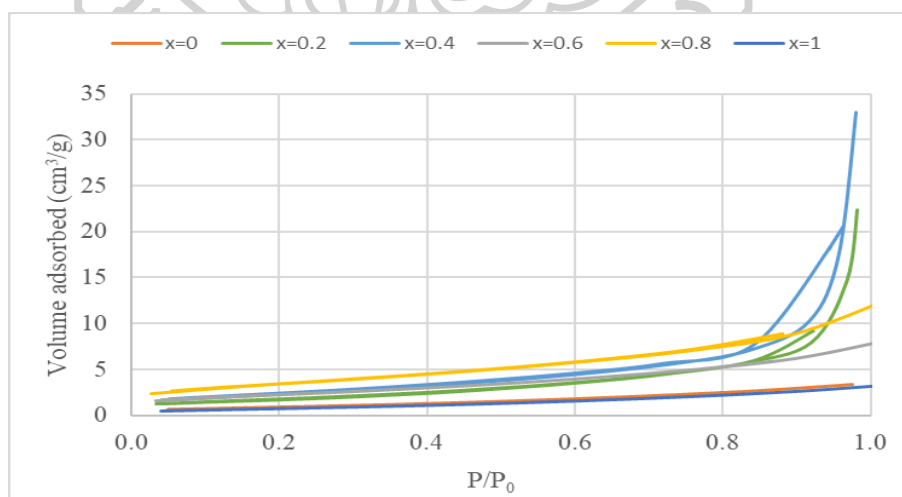
Figure 19 The N_2 adsorption/desorption isotherms of the $2Ni/Ce_xLa_{1-x}CoO_3$ catalysts

The TPR profile for the catalysts different ratio Ce substitutions are shown in Figure 20. The 2Ni/LC catalyst shows the two reduction regions at below and above 500 °C. The first region was assigned as an overlap of three reduction steps. The $LaCoO_3$ was first reduced to form $LaCoO_{2.75}$ and then $La_4Co_3O_{10.}$ The final step shows the reduction of cobalt oxide and nickel oxide. At the region above 500ºC, the reduction of $La_4Co_3O_{10}$ creates La_2O_3 and Co metal. The intensity of the first region was higher when the ratio of Ce/La 0.2, which corresponds with the reduction of Co^{3+} to Co^{2+} and Co^o. This indicates the Ce can be inserted into the perovskite structure and is confirmed with XRD Figure 18a.

For the substitution x=0.40-0.80, the perovskite structure has a lower intensity because the segregated CeO_2, which corresponds with the XRD results (Figure 18a). When, the intensity of the first region was increased respectively it causes the reduction of Co_3O_4 to CoO and CoO to Co metal, confirmed by XPS results (Figure 21). This indicates that increasing the ratio of Ce/La the reduction of cobalt oxides is easier. In second region, it shows the reduction of Ce^{4+} to Ce^{3+}. For the catalyst at x = 1.0 is showed only CeO_2 phases which is confirm by the XRD, the peak at below 500ºC was designed to overlap the reduction of Co^{3+} to Co^{2+} and Co^o
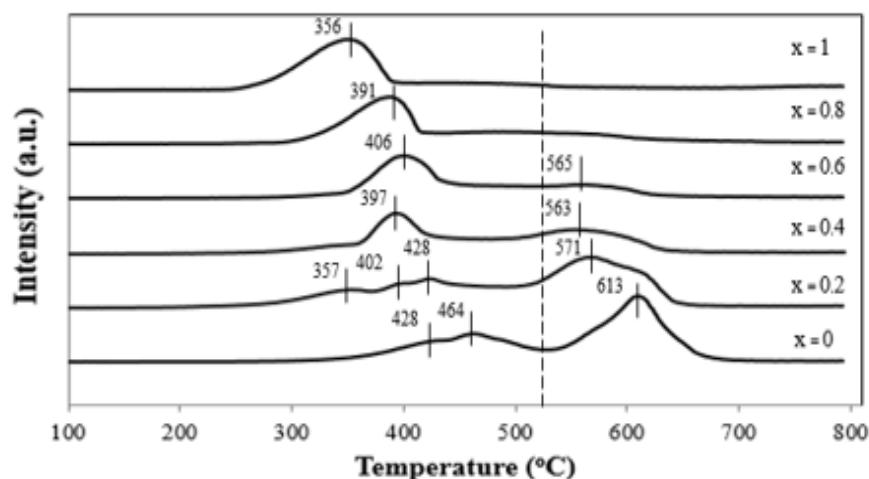

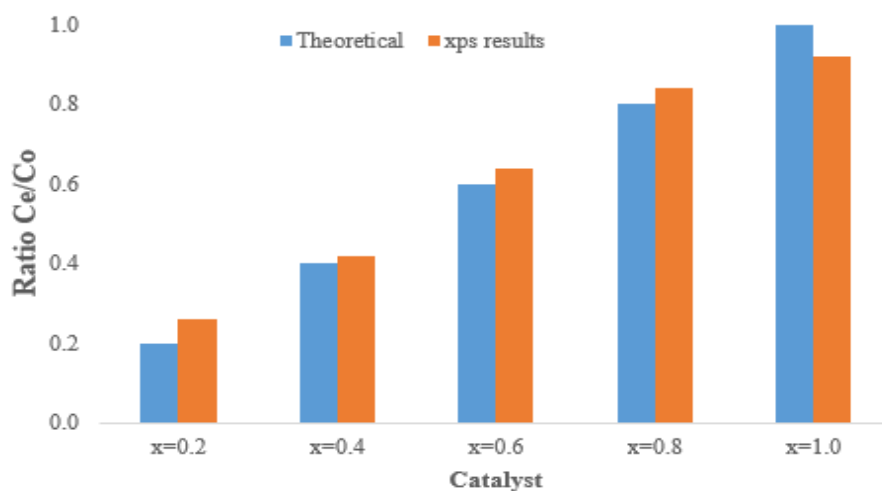**Figure 20** The TPR profile for the catalysts different ratio Ce substitutions

Figure 21 Surface atomic ratios of 2Ni/Ce$_x$La$_{1-x}$CoO$_3$ (x = 0.0-1.0) catalysts

Figure 21 shows the surface atomic ratio of the Ce/Co which was measured by XPS analysis. At a ratio of Ce/Co 0.2-1.0, the ratio in theory is close to the ratio for XPS results. It is confirmed that the cerium was inserted into the perovskite structure. When we increase the ratio of Ce/Co, the Co^{3+} ions decrease, respectively. These results imply that the segregation of the Ce$_2$O phase over the perovskite is due the large ionic radius of Ce^{4+} which is compatible with the XRD results (Figure 18). Figure 21 shows the XPS profile of Ce 3d of 2Ni/Ce$_x$La$_{1-x}$CoO$_3$ (x = 0.2-1.0) catalysts. The eleven peaks were attributed to the Ce$_2$O$_3$ and CeO$_2$ ions in the crystal lattice[56]. At a ratio of Ce/Co 0.2-0.8, the results suggest that the substitution of Ce ions into La ions of 2Ni/LaCoO$_3$ perovskite creates a different size particle of Ce oxide.

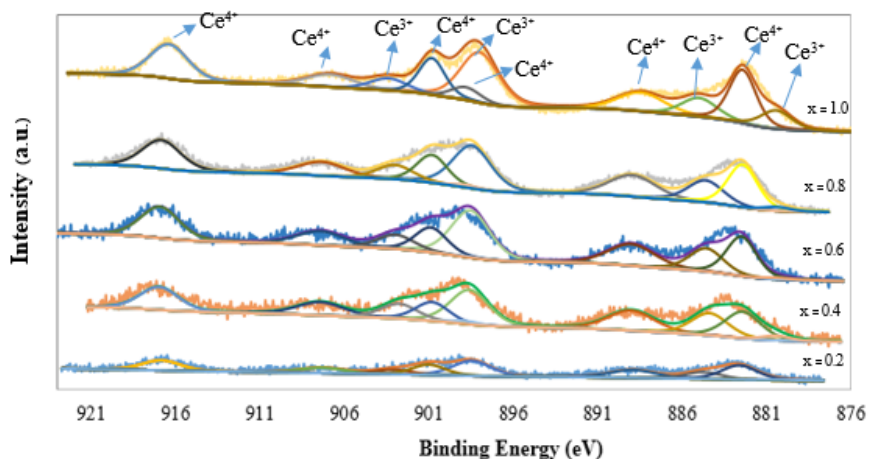**Figure 22** XPS profile of Ce 3d of 2Ni/Ce$_x$La$_{1-x}$CoO$_3$ (x = 0.0-1.0) catalysts

Figure 23 shows the XANES spectra for the $2Ni/Ce_xLa_{1-x}CoO_3$ ($x = 0.0$-1.0) catalysts at Co K-edge. When increase a ratio of Ce/Co led to the reduction of the catalyst, as evident from the shift of the absorption edge to lower energy but higher than that of CoO due to the cobalt has been only partially reduced to Co (II) species[56, 57].
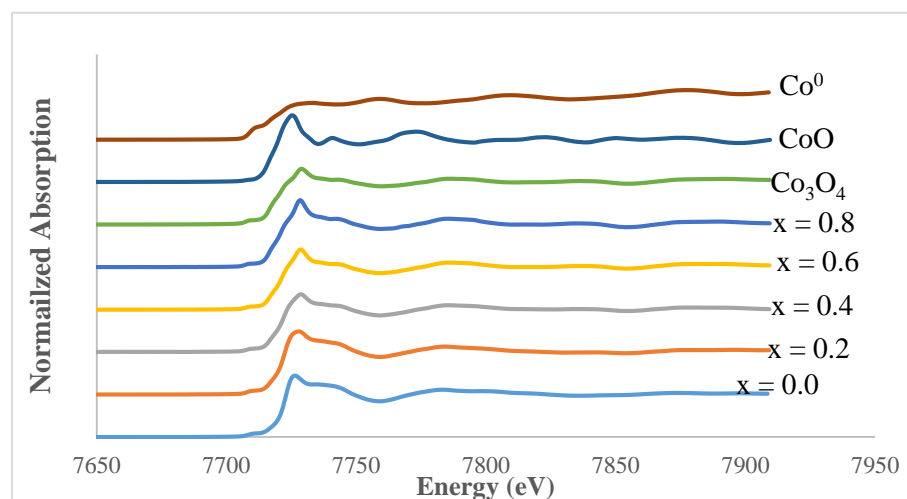

Figure 23 Experimental XANES spectra of $2Ni/Ce_xLa_{1-x}CoO_3$ ($x = 0.0$-1.0) catalysts at Co K-edge

The CH_4 and CO_2 conversions that form the dry reforming reaction at 700°C for 15 h produce various ratios of Ce/Co as shown in Figure 24. At the ratio of Ce/Co 0.0-0.6, it was found that during the conversion of CH_4 and CO_2, the yield of H_2 and CO and the ratio of H_2/CO were relatively unchanged. These results showed that a lower Ce/Co ratio (0.0-0.6) produced a wide spread nickel species dispersion on the La_2O_3 phase. However, when the Ce was inserted into the perovskite, the XRD patterns show the perovskite phase at only x= 0.2. At x= 0.4-0.6, the result did not display a perovskite phase due to small size of the particle with in this phase. The Ni sites were more active than the Co sites in this reaction, therefore the CH_4 was first adsorbed and activated on the surface of the Ni metal. The Ni active sites were well known to promote the reverse water gas shift reaction (RWGS) [50]. This resulted a greater production of CO. While the higher Ce/Co ratio of 0.8 and 1.0 showed a significant increasing of CH_4 and CO_2 conversions, but the yield of H_2 and CO decrease as compared to x= 0.0-0.6. These are the result of the CO methanates side reactions[58].
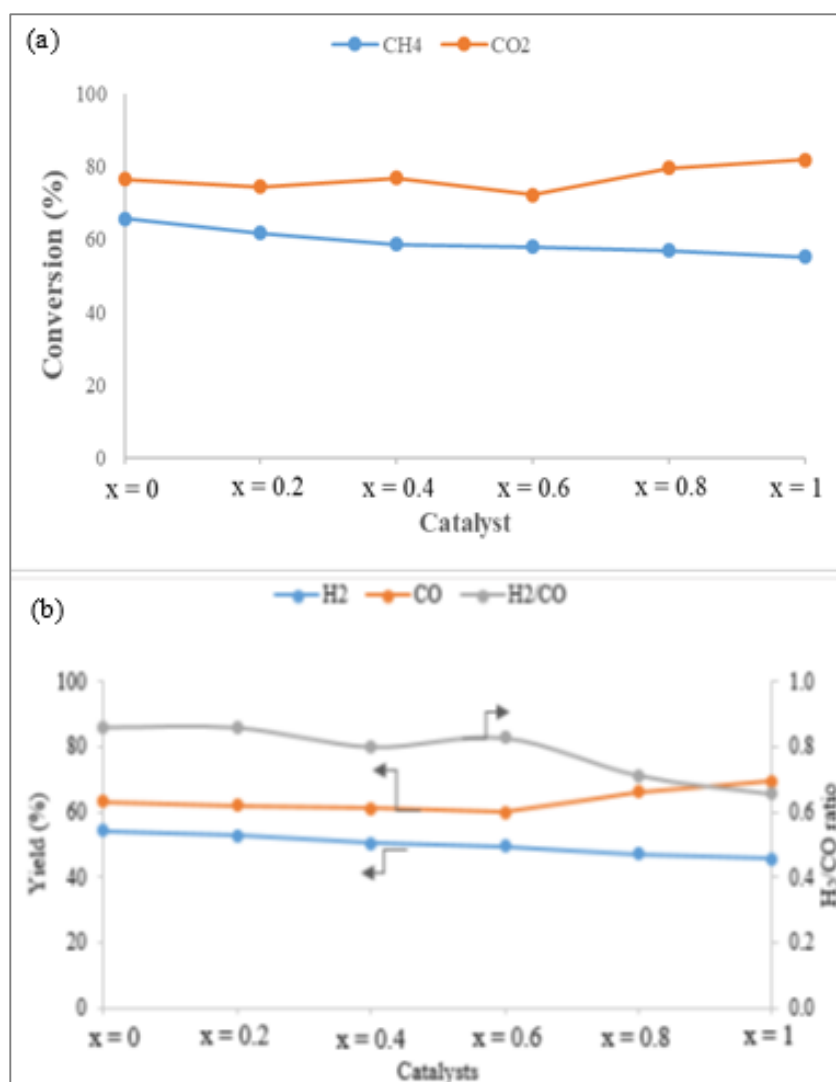
Figure 24 CH_4 and CO_2 conversions at 15 h a) H_2 yiled and b) H_2/CO ratio of 2Ni/$Ce_xLa_{1-x}CoO_3$ (x = 0-1) catalysts in dry reforming of methane at 700 °C for 15 h
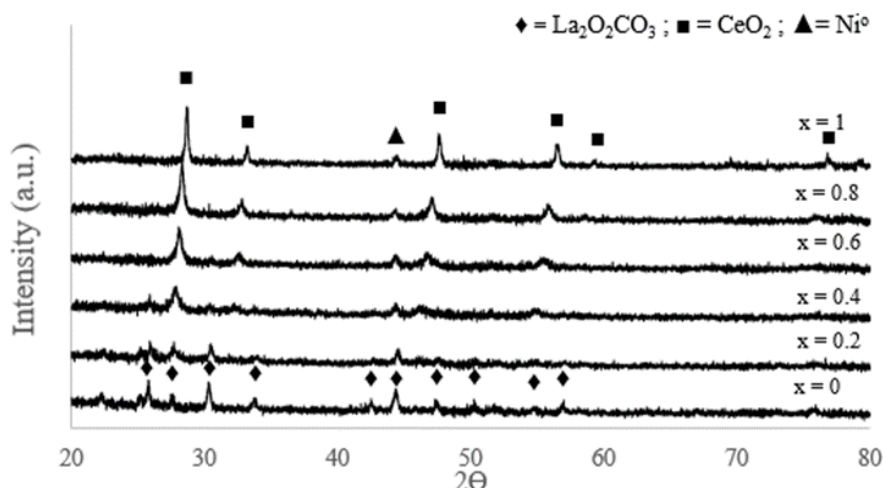
Figure 25 XRD patterns of 2Ni/Ce$_x$La$_{1-x}$CoO$_3$ (x = 0.0-1.0) spent catalysts in dry reforming of methane at 700 °C for 15 h

Figure 25 shows the x-ray diffraction spectra of spent catalysts. The XRD peak at x=0 and x=0.2 were assisgned to be the La$_2$O$_2$CO$_3$ phase due to the La$_2$O$_3$ reacting with the CO$_2$ reactant during the DRM. The XRD peak at x= 0 shows the highest intensity La$_2$O$_2$CO$_3$ phase. This phase can inhibit carbon formation and improve the catalytic activity and stability. When the Ce/Co ratio (0.2-0.8) was increased, the intensity of the La$_2$O$_2$CO$_3$ phase gradually decreased but the CeO$_2$ increased, respectively. These results occurred due to the large size of the CeO$_2$ particles which correspond with table 8. The Ce/Co ratio 1.0 showed the highest intensity of CeO$_2$ phase.
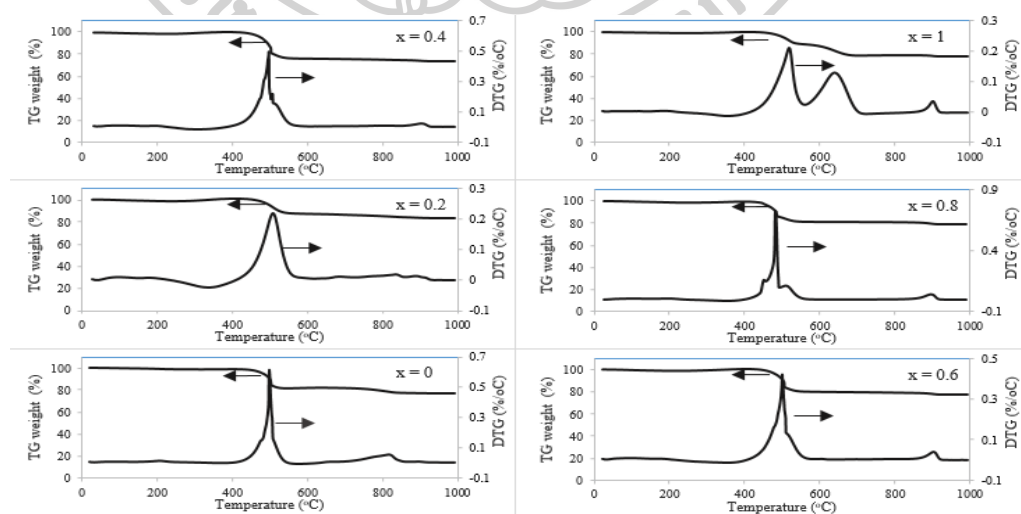

Figure 26 TG and DTG profile of 2Ni/Ce$_x$La$_{1-x}$CoO$_3$ (x = 0-1) spent catalysts in dry reforming of methane at 700 °C for 15 h

Figure 26 shows the weight loss and derivative weight loss of all spent catalysts obtained after DRM reaction at 700 °C for 15 h were investigated by using TGA. At x= 0.0-0.8, it showed two major steps of decomposition. The first steps occurred in the range of 300 and 550 °C. This weight loss has been attributed to the oxidation of the amorphous carbon, which is the active species in the formation of synthesis gas. The second weight loss about 800 °C has been attributed to the decomposition of La carbonates. The weight loss of all catalysts show range of 16-27 % weight loss. The weight loss comparison can be seen in table 8. The Ce/Co ratio 1.0 shows revealed another shoulder in the range of 400-500 °C. Inaddition, the lower-temperature (300-500°C) and higher-temperature (800-900°C) peaks can be assigned to the CH_x species and carbon filaments, respectively [59]. Coke deposition with DTA peak at higher temperature causes the catalyst deactivation.

Table 8 The weight loss of $2Ni/Ce_xLa_{1-x}CoO_3$ (x = 0.0-1.0) catalysts

Catalyst	Weight loss TG after reaction(%)
x= 1.0	22.0
x = 0.8	20.8
x = 0.6	21.8
x = 0.4	26.7
x = 0.2	16.5
x = 0.0	23.2

4.3 Effect of the transition metals substitution into Co position

Figure 27 shows the x-ray diffraction spectra of the transition metals substitution into Co position. The perovskite structures were formed when using Mn metal but they did not forme when using Zn and Cu metal. The $2Ni/LaMnO_3$ catalyst decreases the intensity of the perovskite peaks when compared to the $2Ni/LaCoO_3$ catalyst. The $2Ni/LaCuO_3$ shows La_2CuO_4 spinel and CuO phase. The La_2CuO_4 is a perovskite-like type mixed oxide which is composed of alternating layers of $(LaO)_2$ rock salt and the caxis CuO_2 sheet. The catalytic properties of La_2CuO_4 also make it useful in various oxidation and reduction reactions. In addition, it has great potential to be used as electrode materials[60]. The $2Ni/LaZnO_3$ shows a mixed phase of La_2O_3, ZnO and $La(OH)_3$.
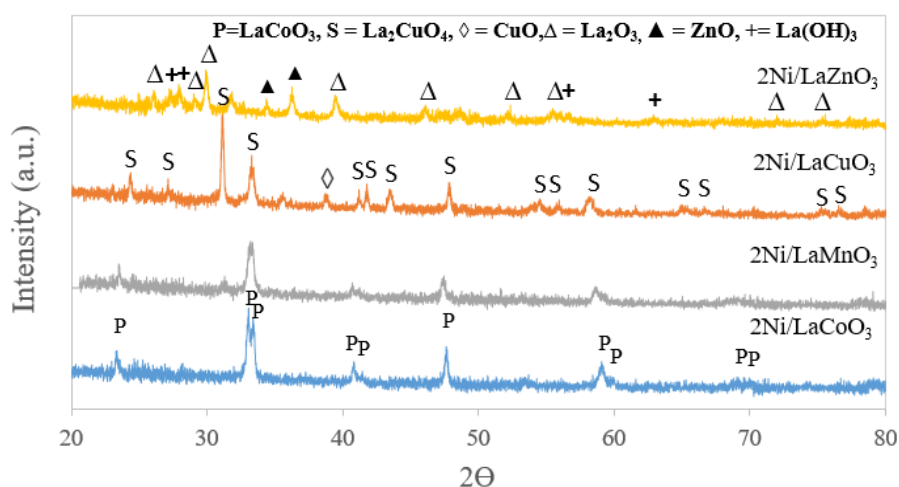
Figure 27 XRD patterns of 2Ni/LaBO$_3$ (B = Co, Mn, Zn and Cu) catalysts

The catalysts show BET surface area, ranging of 3.4 to 12.8 m^2/g. The 2Ni/LaMnO$_3$ catalyst shows the highest surface area at 12.8 m^2/g. When loading Mn, Cu and Zn metal, they increase the pore size diameter when compared to the 2Ni/LaCoO$_3$ catalyst. The BET surface area, pore size diameter and pore volume are shown table 9.

Table 9 The BET surface area(S$_{BET}$), the average pore diameter and pore volume

Catalyst	S$_{BET}$ (m^2/g)	Pore size (nm)	Pore volume (cm^3/g)
2Ni/LaCoO$_3$	3.4	6.1	0.005
2Ni/LaMnO$_3$	12.8	23.4	0.075
2Ni/LaCuO$_3$	3.3	19.8	0.016
2Ni/LaZnO$_3$	8.4	16.4	0.036

The TPR profile for the catalysts different transition metals are shown in Figure 28. The $2Ni/LaCoO_3$ catalyst shows the two reduction regions at below and above 500 °C. When replaced with Mn, Zn and Cu metals, the degree of reducibility decrease when compared to the $2Ni/LaCoO_3$ catalyst. The $2Ni/LaMnO_3$ catalyst shows two reduction regions. The lower temperature region (250-350 °C) was assigned to the reduction of Mn^{4+} to Mn^{3+}. The higher temperature region (650-800 °C) was assigned to the reduction of Mn^{3+} to Mn^{2+}[61]. The $2Ni/LaCuO_3$ displays in two reduction regions, at 210 - 314 °C and 500 °C which results in the reduction of Cu^{3+} to Cu^+. The second reduction region was completely reduced Cu^+ to Cu metal [62]. The major reduction peaks obviously shift toward lower temperatures with the increasing amount of Cu mole fraction indicating that doping Cu and La_2Cuo_4 production would improve the sorbent reducibility.
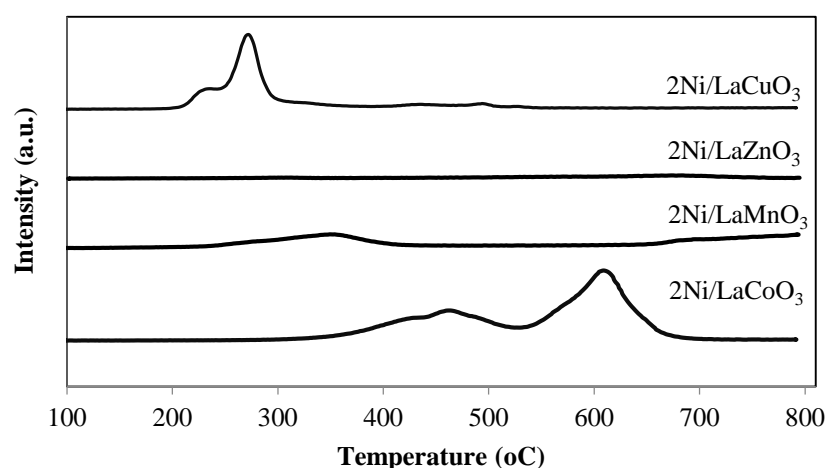

Figure 28 TPR profiles of $2Ni/LaBO_3$ (B = Co, Mn, Zn and Cu) catalysts

From the DRM reaction results nas shown in Figure 29. The $2Ni/LaCoO_3$ catalyst shows the highest activity during the reaction and a higher conversion of CO_2 than CH_4 due to the effect of the RWGS reaction. The XRD pattern of the after-reaction shows the $La_2O_2CO_3$ phase. This phase inhibits carbon formation and improves the catalytic activity and stability. The $2Ni/LaMnO_3$ catalyst shows a higher CH_4 and CO_2 conversion when compared with the Zn and Cu metal. In addition, it also shows the perovskite phase and is confirmed with XRD Figure 27. The Mn/Co ratio at 0.05 shows the highest CH_4 conversion, H_2 yield and H_2/CO ratio. The Mn and Co mix metals increase catalytic activity due to a change in oxygen mobility within the crystal lattice of the Co component. The Mn/Co ratio at 0.1-0.5 show a decrease in the CO_2 and CH_4 conversion after the 9 hr mark due to metals sintering.
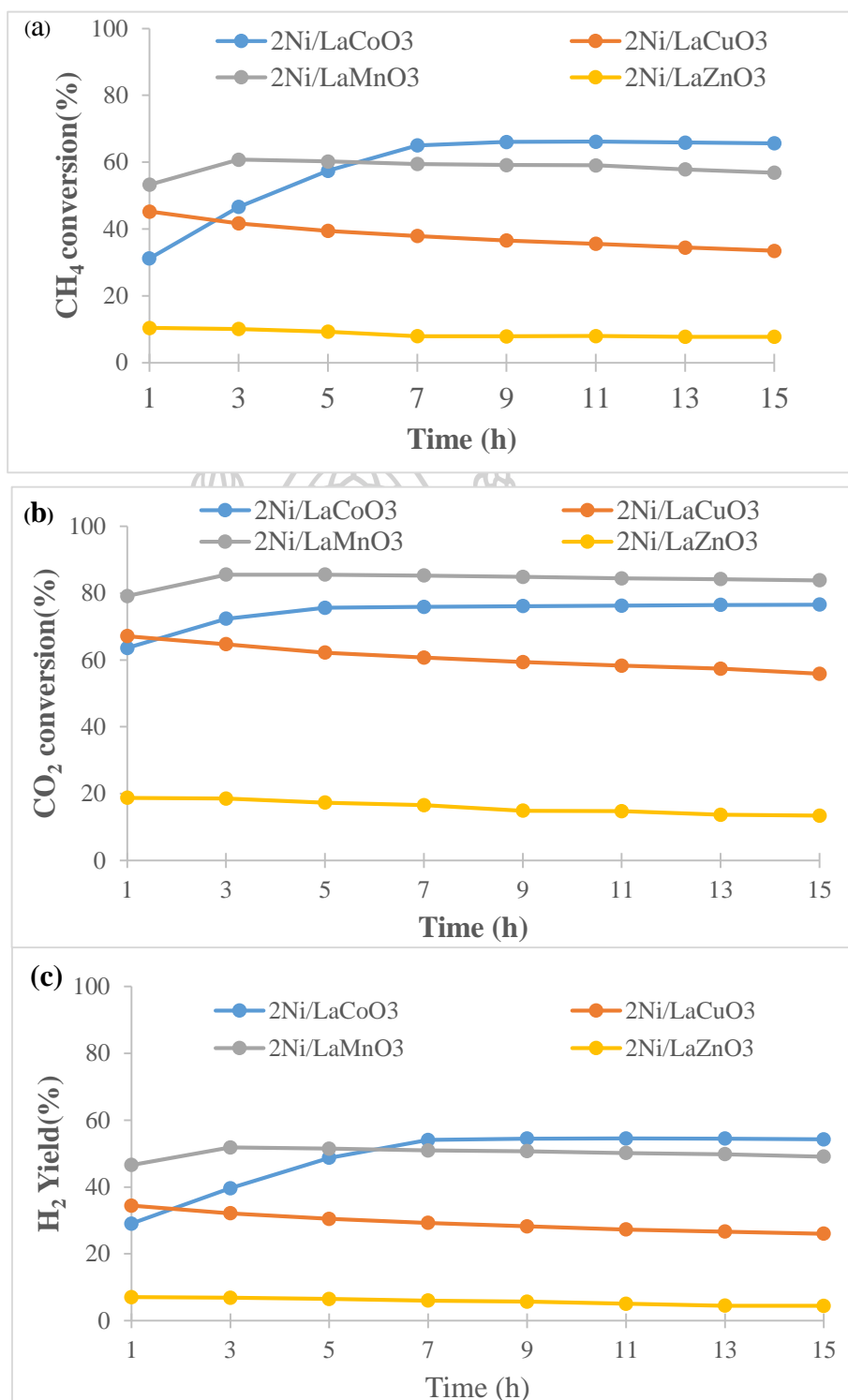
Figure 29 CH_4 and CO_2 conversions at 15 h a) H_2 yiled and b) H_2/CO ratio of the catalysts different transition metals in dry reforming of methane at 700 °C for 15 h

Since, the Mn metal substitution into Co metal shows maintain perovskite structure and show high CH_4 and CO_2 conversion when compare with the Zn and Cu metal. So, the effect of partial Mn metal substitution into Co metal was studied. Figure 30 shows XRD patterns of $2Ni/LaMn_yCo_{1-y}O_3$ catalysts (y = 0.0, 0.05, 0.1, 0.5 and 1.0). For all catalyst show the perovskite peak. The Mn/Co ratio 0.05 shows the same perovskite peaks with the Mn/Co ratio 0.0. The Mn/Co ratio 0.1-0.5 shows same dominant peaks with the Mn/Co ratio 1.0
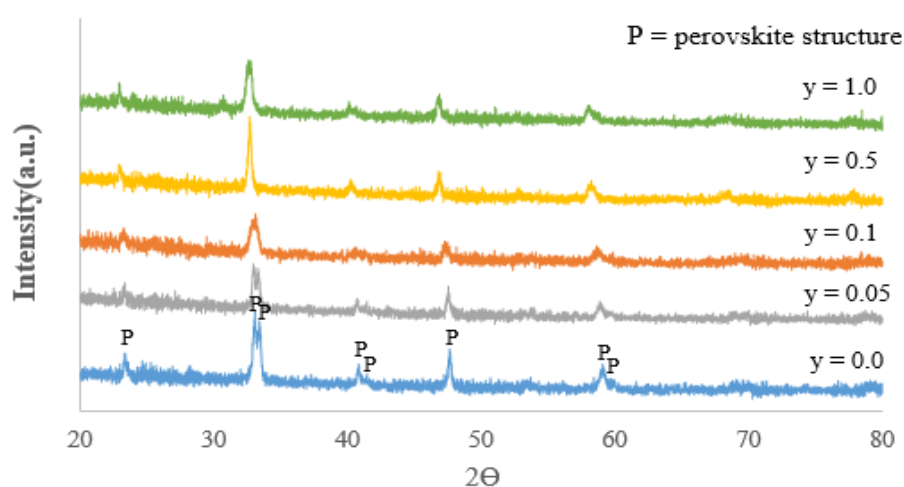

Figure 30 XRD patterns of $2Ni/LaB_yCo_{1-y}O_3$ catalysts (y = 0.0, 0.05, 0.1, 0.5 and 1.0)

The TPR profile of $2Ni/LaB_yCo_{1-y}O_3$ catalysts (y = 0.0, 0.05, 0.1, 0.5 and 1.0) are shown in Figure 31. The Mn/Co ratio 0.0 and 0.05 show the two reduction regions at below and above 500 °C. The first region was assigned as an overlap of three reduction steps. The $LaCoO_3$ was first reduced to form $LaCoO_{2.75}$ and then $La_4Co_3O_{10}$. The final step shows the reduction of cobalt oxide and nickel oxide. At the region above 500°C, the reduction of $La_4Co_3O_{10}$ creates La_2O_3 and Co metal. The Mn/Co ratio 0.5 and 1.0 show two reduction regions. The lower temperature region (250-350 °C) was assigned to the reduction of Mn^{4+} to Mn^{3+}. The higher temperature region (650-800 °C) was assigned to the reduction of Mn^{3+} to Mn^{2+}. At Mn/Co ratio 0.1 show the characteristic of reduction properties same both Co and Mn pure.
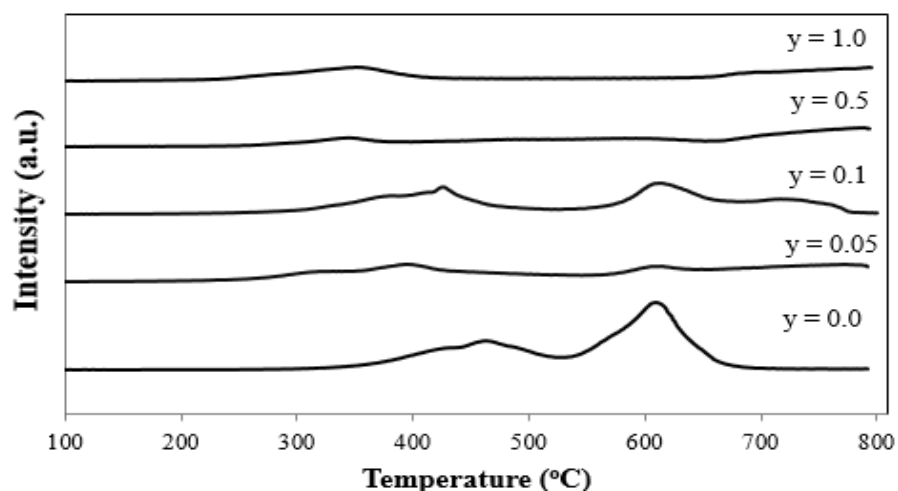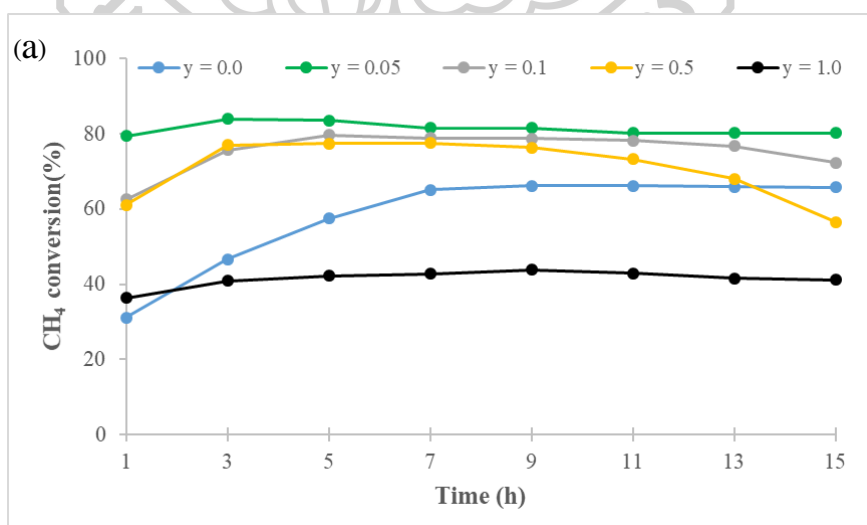
Figure 31 TPR profiles of $2Ni/LaB_yCo_{1-y}O_3$ catalysts (y = 0.0, 0.05, 0.1, 0.5 and 1.0)

Figure 32 shows result DRM synthesis. The Mn/Co at 0.05 ratio shows the highest CH_4 conversion, H_2 yield and H_2/CO ratio. When increase the Mn/Co ratio at 0.1, the CH_4 conversion slightly decrease and is significant after 13 h. At Mn/Co ratio 0.5, the CH_4 and CO_2 conversion decreased significantly after 9 h due to it occur the catalyst deactivate. The Mn and Co mix metals increase catalytic activity due to a change in oxygen mobility within the crystal lattice of the Co component.
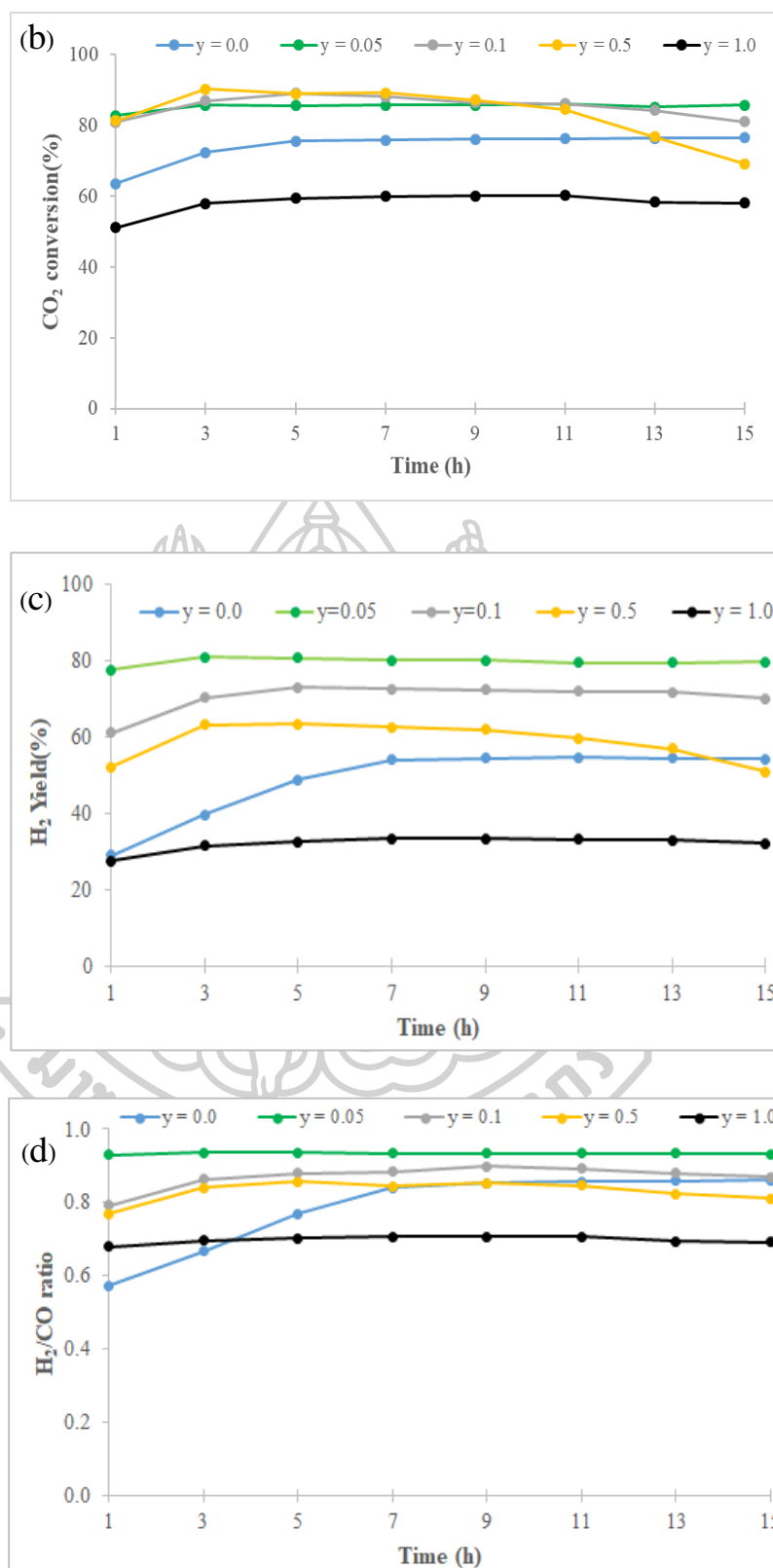
Figure 32 CH$_4$ conversion a) CO$_2$ conversion b) H$_2$ yiled c) and H$_2$/CO ratio d) of 2Ni/LaB$_y$Co$_{1-y}$O$_3$ catalysts (y = 0.0, 0.05, 0.1, 0.5 and 1.0) in dry reforming of methane at 700 °C for 15 h

Figure 33 shows TG and DTG profile of 2Ni/LaMn$_y$Co$_{1-y}$O$_3$ catalysts (y = 0.0, 0.05, 0.1, 0.5 and 1.0)) spent catalysts in dry reforming of methane at 700 °C for 15 h. All of the Mn/Co ratio, it showed two major steps of decomposition. The first steps occurred in the range of 300 and 550 °C. This weight loss has been attributed to the cabonatation step of the La$_2$O$_2$CO$_3$ formation, which is the active species in the formation of synthesis gas. The second weight loss about 800 °C has been attributed to the decomposition of La carbonates. The weight loss comparison can be seen in table 10. The weight loss of y=0.05 show the lowest weight loss at 18.4 %. The Mn/Co at 0.1 and 0.5 show a high weigt loss. This causes shows show a decrease in the CO$_2$ and CH$_4$ conversion after the 9 hr mark.
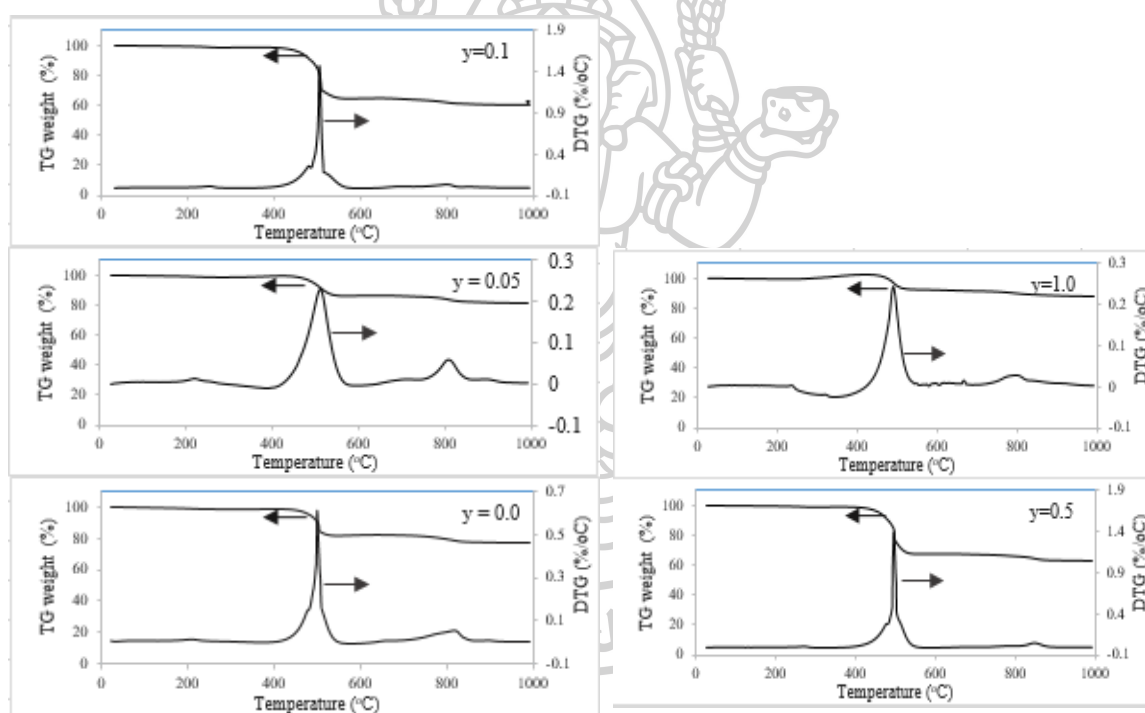

Figure 33 TG and DTG profile of 2Ni/LaMn$_y$Co$_{1-y}$O$_3$ catalysts (y = 0.0, 0.05, 0.1, 0.5 and 1.0)) spent catalysts in dry reforming of methane at 700 °C for 15 h

Table 10 The weight loss of $2Ni/LaMn_yCo_{1-y}O_3$ catalysts $(y = 0.0, 0.05, 0.1, 0.5$ and $1.0)$ catalysts

Catalyst	Weight loss TG after reaction(%)
y = 0.0	23.2
y = 0.05	18.4
y = 0.1	36.7
y = 0.5	37.1
y = 1.0	12.3

CHAPTER V
CONCLUSIONS AND RECOMMENDATION

The results and discussion in this chapter are divided into three parts, the effect of Ni loading, the Ce partial substitution into La position and the transition metal (Cu, Mn and Zn) substitution into Co position.

5.1 Conclusions

5.1.1   The effect of Ni loading on LaCoO$_3$ perovskites

The result of FSP method and calcined condition affects the formation of LaCoO$_3$ perovskite structure. However, Ni loading by impregnation method maintains the perovskite structure but decreases the degree of its crystallinity. The 2Ni/LC show highest reducibility. The LC catalyst shows poor CH$_4$ and CO$_2$ conversions due to the reduction temperature to 500°C which was not enough to produce the Co metal dispered in the La$_2$O$_3$ support. When increasing the Ni loading by 2, 5 and 10 wt%, they show high activity for the reaction and a higher conversion of CO$_2$ than CH$_4$. The H$_2$/CO ratio is less than 1 and results in the reverse water gas shift side reaction (RWGS). The result of 2Ni/LC show the highest CH$_4$ and CO$_2$ conversion. For the XRD pattern of the spent catalysts, it showed the highest intensity La$_2$O$_2$CO$_3$ phase. This phase removes carbon formation on the surface catalyst. For role nickel when adding more than 2 wt.%, it decreases the loading of the perovskite structure due to higher amounts of Ni loading and a larger amount of sintering Ni metal. This causes low activity and an increase in the RWGS

5.1.2   The effect of Ce partial substitution into La position

The 2Ni/Ce$_x$La$_{1-x}$CoO$_3$ (x = 0.0, 0.2, 0.4, 0.6, 0.8 and 1.0) were investigated. The XRD analyses confirmed that at Ce contents x = 0.2 maintained the perovskite structure but decreases the degree of its crystallinity. Which the insertion of Ce 0.4 and 0.6, the XRD pattern appear as segregated CeO$_2$ phase and interferes with the rate of perovskite structure formation. When increasing Ce to 0.8 and 1.0, they show CeO$_2$ and CoO$_3$ phase. The substitution of the La site metal ion with Ce metal ion at x= 0.2, 0.4 and 0.6 show little change in the CO$_2$ and CH$_4$ conversion. When increase to x=0.8 and 1.0 show slight increase CH$_4$ and CO$_2$ conversion but obvious decrease in H$_2$ and

CO yield due to the effect of RWGS reaction. Its insertion in the perovskite structure is also possible in the low Ce-content.

5.1.2   The transition metal substitution into Co position.

The perovskite structures were formed when using Co and Mn metals but they did not forme when using Zn and Cu metal. The BET surface area of catalysts show range of 3.4 to 12.8 m^2/g. The $2Ni/LaMnO_3$ catalyst shows the highest surface area at 12.8 m^2/g. The $2Ni/LaMnO_3$ catalyst decreases the intensity of the perovskite peaks when compared to the $2Ni/LaCoO_3$ catalyst. The $2Ni/LaCuO_3$ shows La_2CuO_4 spinel and CuO phase. The $2Ni/LaZnO_3$ shows a mixed phase of La_2O_3, ZnO and $La(OH)_3$. All of the Mn/Co ratio maintains the perovskite structure. The conversion of CH_4 and CO_2, the yield of H_2 and CO and the ratio of H_2/CO show: $2Ni/LaCoO_3 > 2Ni/LaMnO_3 > 2Ni/LaCuO_3 > 2Ni/LaZnO_3$, respectively. The Mn/Co ratio at 0.05 shows the highest CH_4 conversion, H_2 yield and H_2/CO ratio. The Mn metal partial replacement at the Co sites can increase catalytic activity due to a change in oxygen mobility within the crystal lattice of the Co component. The Mn/Co ratio at 0.1-0.5 show a decrease in the CO_2 and CH_4 conversion after the 9 hr mark due to metals sintering.
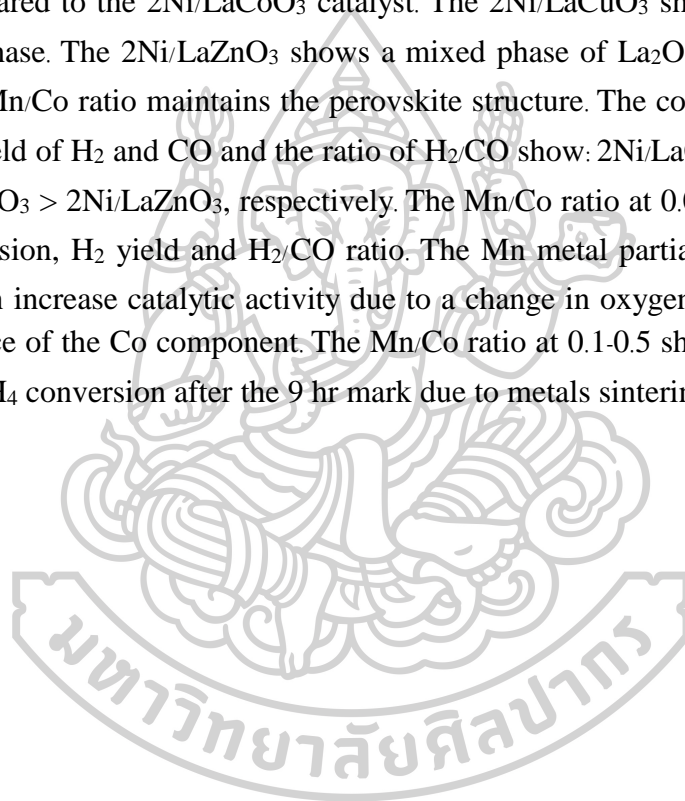
APPENDIX A

CALCULATION FOR CATALYST PREPARATION

Table A.1 Chemical Properties

Metal or Metal oxide	MW of metal	Formula	MW of Metal Precursor	Metal content (%)
La_2O_3	325.8	$LaN_3O_9 \cdot 6H_2O$	432.4	99
Ce_2O_3	328.2	$Ce(NO_3)_3 \cdot 6H_2O$	434.2	99
Co	58.9	$Co(NO_3)_2 6H_2O$	290.9	98
Mn	54.9	$Mn(NO_3)_2 4H_2O$	250.9	99
Cu	63.5	$Cu(NO_3)_2 \cdot 3H_2O$	241.6	98
Zn	65.4	$Zn(NO_3)_2 \cdot 6H_2O$	297.4	98

Calculation of catalyst prepared by flame spray pyrolysis

0.5 M solution was used as precursor for catalyst preparation by flame spray pyrolysis is shown as follows:

Example: Calculation for the preparation of the $LaCoO_3$ catalysts, 70 wt% of Lanthanum (III) nitrate hexahydrate and 30 wt% cobalt nitrate were used as precursor and diluted with ethanol to a 0.5 M in 300 ml of solution

$$\text{Mole precursor} = 300 ml \left| \frac{0.1 mole}{1000 ml} = 0.15 mole \right.$$

$$\text{Mole Co} = \frac{30.00}{58.93} = 0.509 \text{ mole Co}$$

$$\text{Mole La}_2O_3 = \frac{70.00}{325.82} \times 2 = 0.430 \text{ mole La}_2O_3$$

Total mole $= 0.509 + 0.430 = 0.939$ mole

$$\therefore \text{Co(NO}_3)_2.6\text{H}_2\text{O} \quad = \quad \frac{0.15\,mole}{0.98} \left| \frac{0.509\,mole}{0.939\,mole} \right| \frac{290.9\,g}{mole} \quad = \quad 24.136 \qquad \text{g}$$

$$\therefore \text{LaN}_3\text{O}_9 \cdot 6\text{H}_2\text{O} \quad = \quad \frac{0.15\,mole}{0.99} \left| \frac{0.430\,mole}{0.939\,mole} \right| \frac{432.91\,g}{mole} \quad = \quad 30.036 \qquad \text{g}$$

APPENDIX B

CALCULATION OF THE CRSTALLITE SIZE

Calculation of the crystallite size by Debye-Scherrer equation

The crystallite size was calculated from the half-height width of the diffraction peak of XRD pattern using the Debye-Scherrer equation.
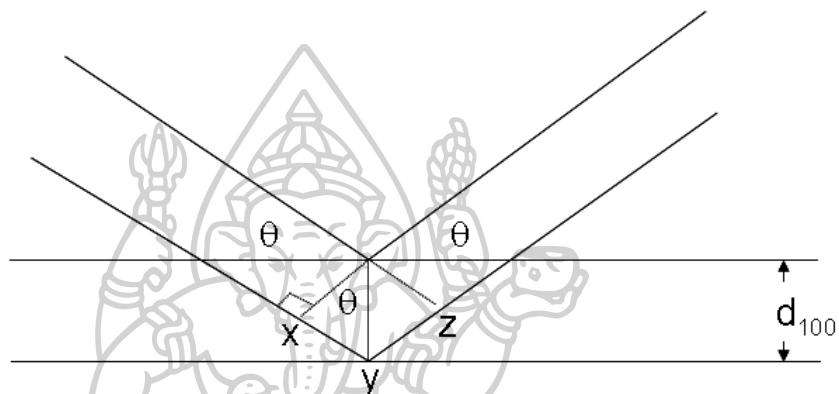

Figure B.1　Derivation of Bragg's Law for X-ray diffraction

$$xy = yz = d\sin\theta$$

Thus　　　　　　　　　　$$xyz = 2d\sin\theta$$

But　　　　　　　　　　$$xyz = n\lambda$$

Therefore　　　　　　　$$2d\sin\theta = n\lambda$$

Bragg's Law　　　　　　$$d = \frac{n\lambda}{2\sin\theta}$$

The Bragg's Law was derived to B.1

From Scherrer equation:

$$D = \frac{K\lambda}{\beta\cos\theta} \qquad\qquad (B.1)$$

Where   D = Crystallite size, Å

K = Crystallite-shape factor = 0.9

λ = X-ray wavelength, 1.5418 Å for CuKα

θ = Observed peak angle, degree

β = Full-width at Half-Maximum (FWHM), radian

From Warren's formula:

$$\beta = \sqrt{B_M^2 - B_S^2} \qquad (B.2)$$

Where B_M = The measured peak width in radians at half peak height.

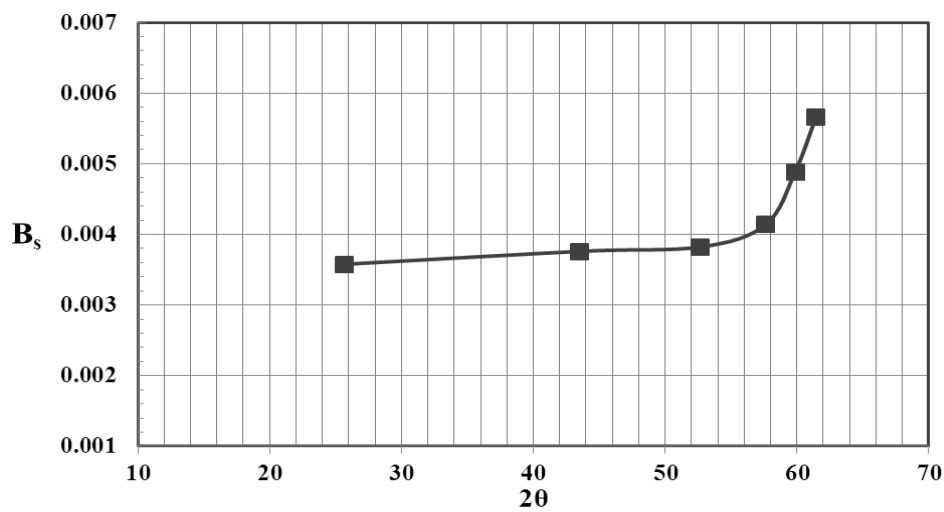B_S = The corresponding width of the standard material.

Figure B.2   The standard width of reference α-alumina sample

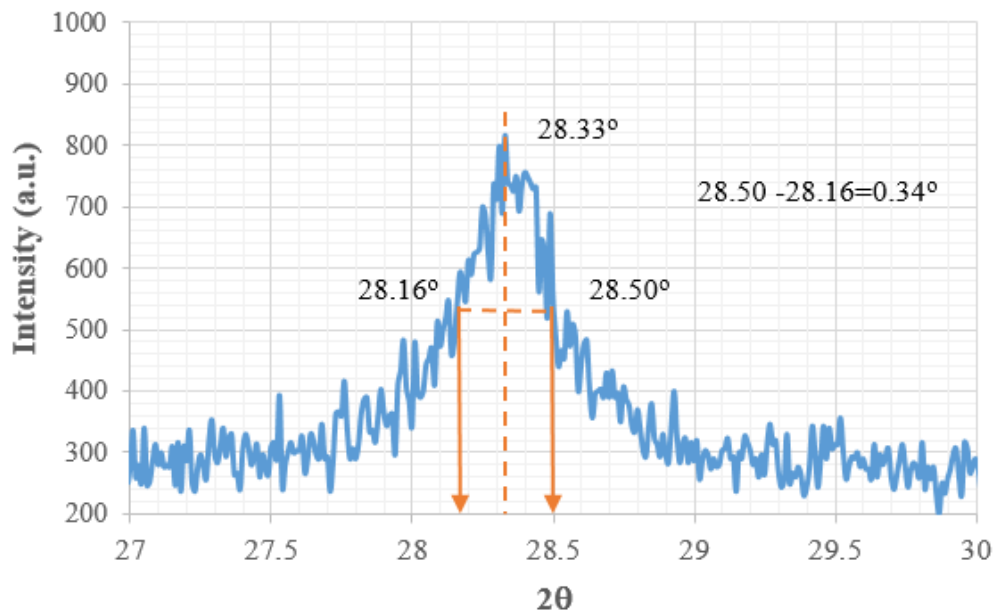**Example: Calculation of the crystallite size of 2Ni/Ce$_x$La$_{1-x}$CoO$_3$ (x = 0.8) catalysts**

Figure B.3 The half-height width of 2Ni/Ce$_x$La$_{1-x}$CoO$_3$ (x = 0.8) catalysts at 28.33°.

The half-height width of 111 diffraction peak = 0.34° (from Figure A.3)

$$= 0.34 \times \frac{\pi}{180}$$

$$= 0.005931 \text{ radian}$$

The corresponding half-height width of peak of α-alumina (from the B$_s$ value at the 2θ of 28.33° in Figure A.2) = 0.0037 radian

The peak width, $\beta = \sqrt{B_M^2 - B_S^2}$

$$= \sqrt{0.005931^2 - 0.0037^2}$$

$$= 0.00464 \text{ } radian$$

$2\theta \quad = \quad 28.33°$

$\theta \quad = \quad 14.165°$

$$\lambda \quad = \quad 1.5418 \ \text{Å}$$

The crystallite size $\quad = \dfrac{0.9 \times 1.5418}{0.00464 \cos 14.165} \quad = 308.4 \ \text{Å} = 30.84 \ \text{nm}$

APPENDIX C

N₂ ADSORTION/DESORPTION ISOTHERMS AND PORE SIZE
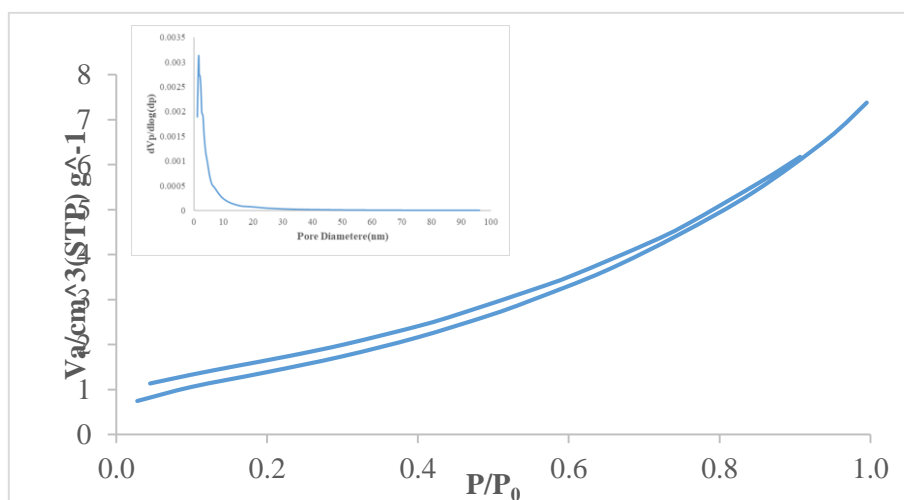
DISTRIBUTION

Figure C.1 The N_2 adsorption/desorption isotherms and the pore size distribution of the $LaCoO_3$ catalysts
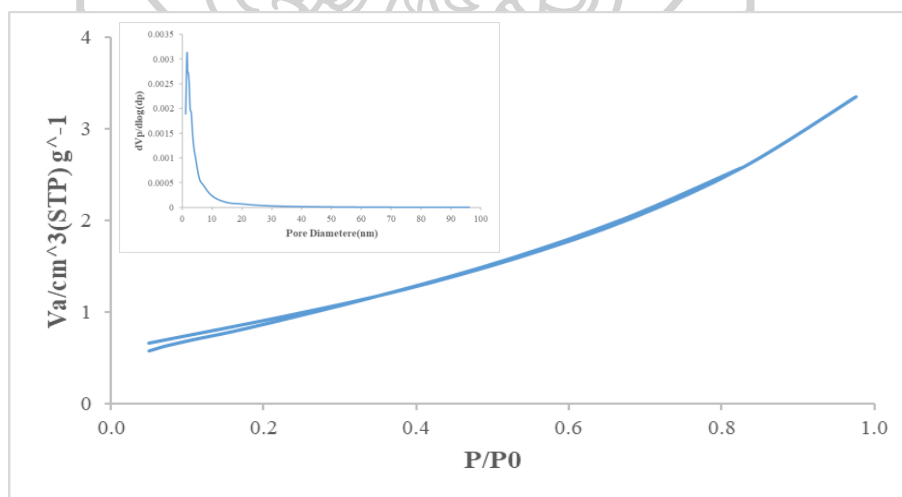

Figure C.2 The N_2 adsorption/desorption isotherms and the pore size distribution of the 2Ni/LC catalysts
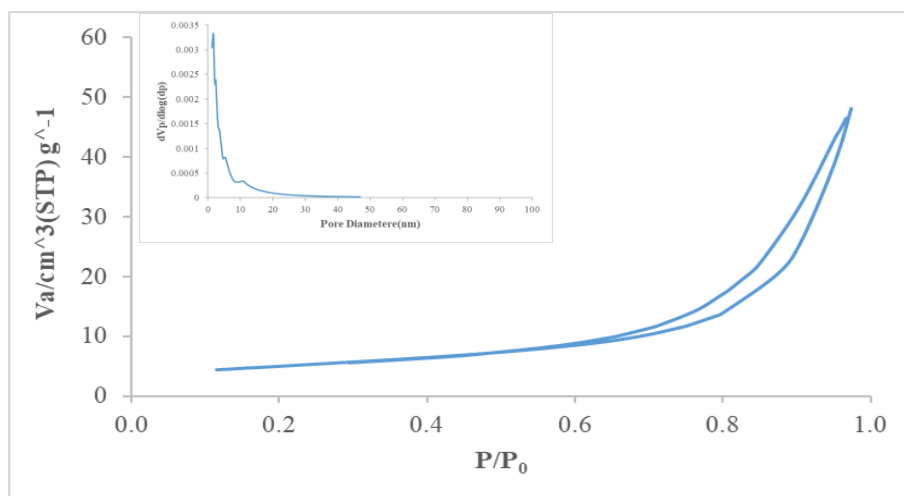
Figure C.3 The N_2 adsorption/desorption isotherms and the pore size distribution of the 5Ni/LC catalysts
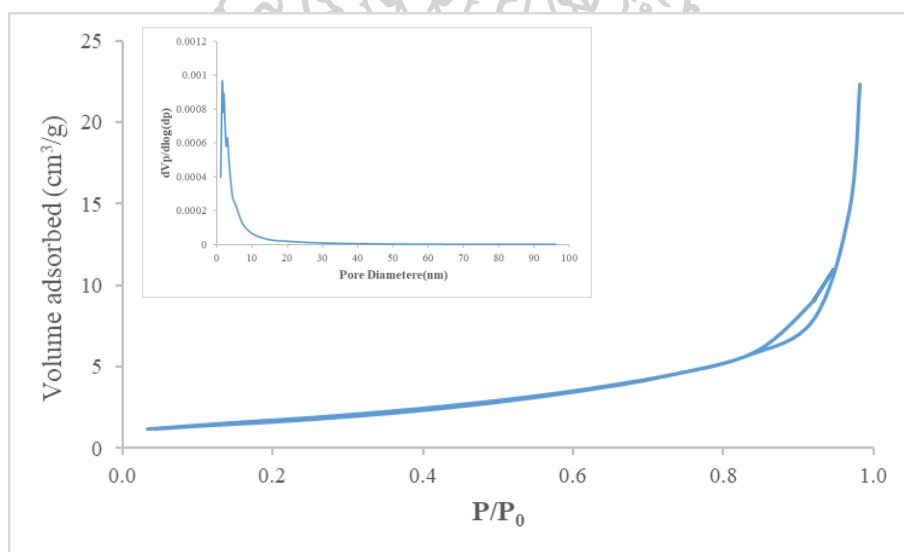

Figure C.4 The N_2 adsorption/desorption isotherms and the pore size distribution of the 10Ni/LC catalysts
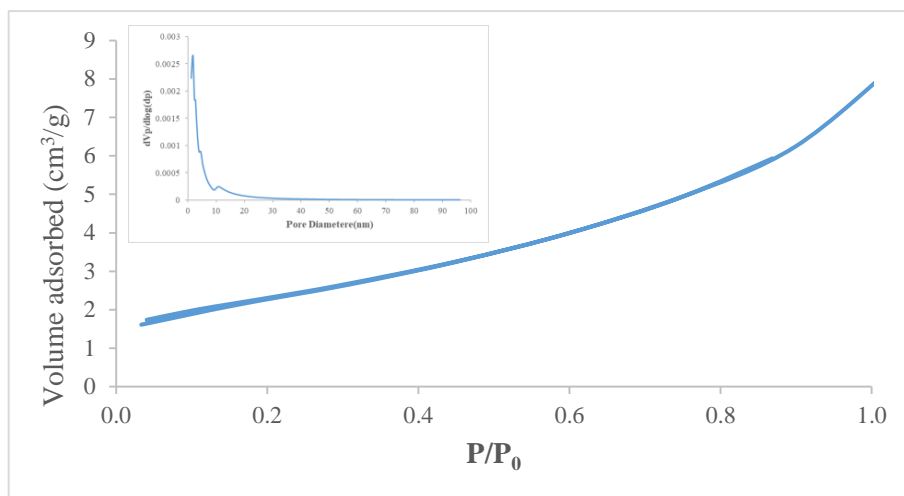
Figure C.5 The N_2 adsorption/desorption isotherms and the pore size distribution of the 2Ni/$Ce_{0.2}La_{0.8}CoO_3$catalysts

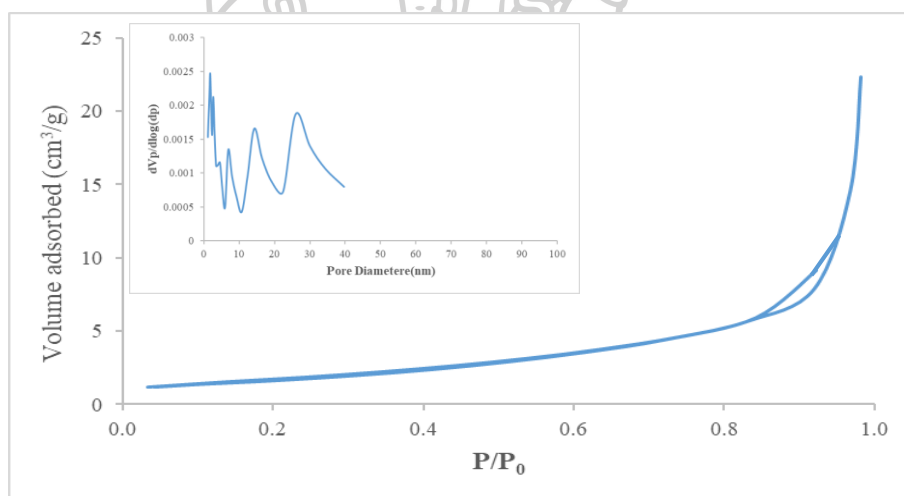

Figure C.6 The N_2 adsorption/desorption isotherms and the pore size distribution of the 2Ni/$Ce_{0.4}La_{0.6}CoO_3$catalysts

Figure C.7 The N_2 adsorption/desorption isotherms and the pore size distribution of the 2Ni/Ce$_{0.6}$La$_{0.4}$CoO$_3$catalysts

Figure C.8 The N_2 adsorption/desorption isotherms and the pore size distribution of the 2Ni/Ce$_{0.8}$La$_{0.2}$CoO$_3$catalysts
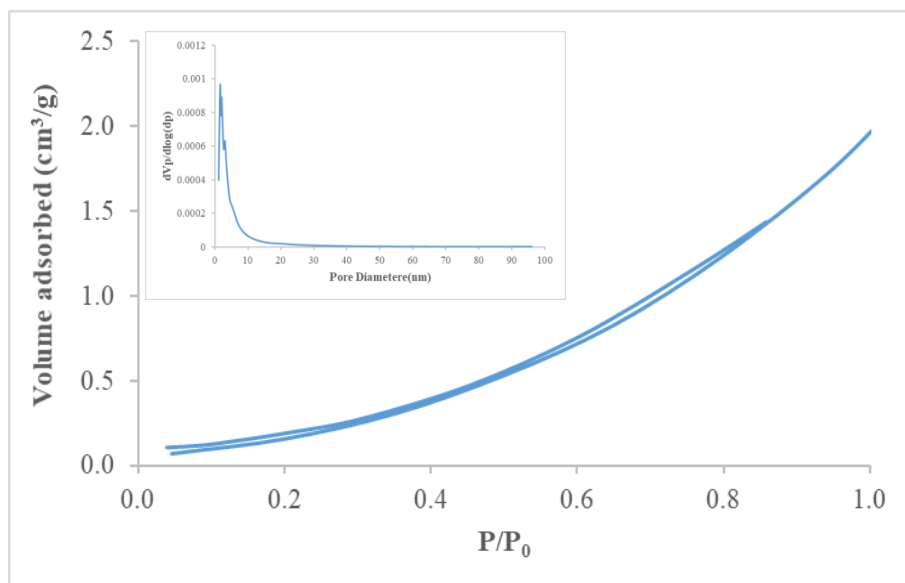
Figure C.9 The N_2 adsorption/desorption isotherms and the pore size distribution of the 2Ni/CeCoO$_3$catalysts

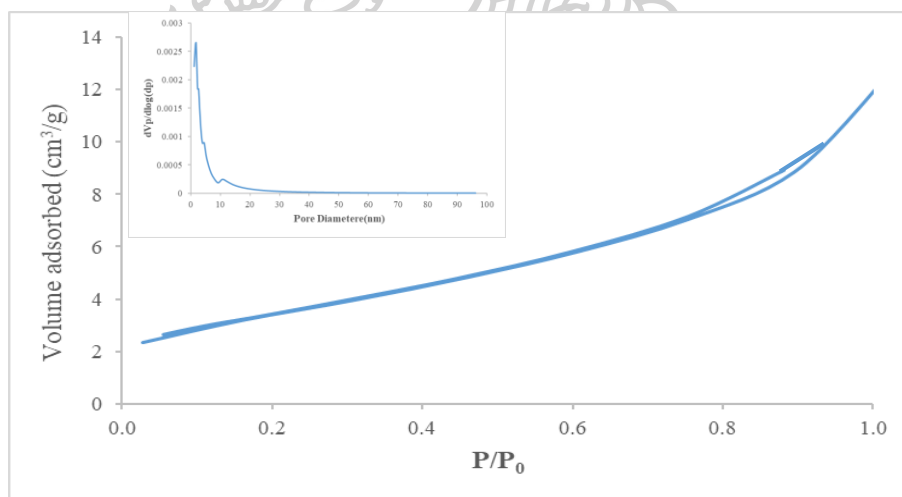Figure C.10 The N_2 adsorption/desorption isotherms and the pore size distribution of the 2Ni/LaMnO$_3$catalysts
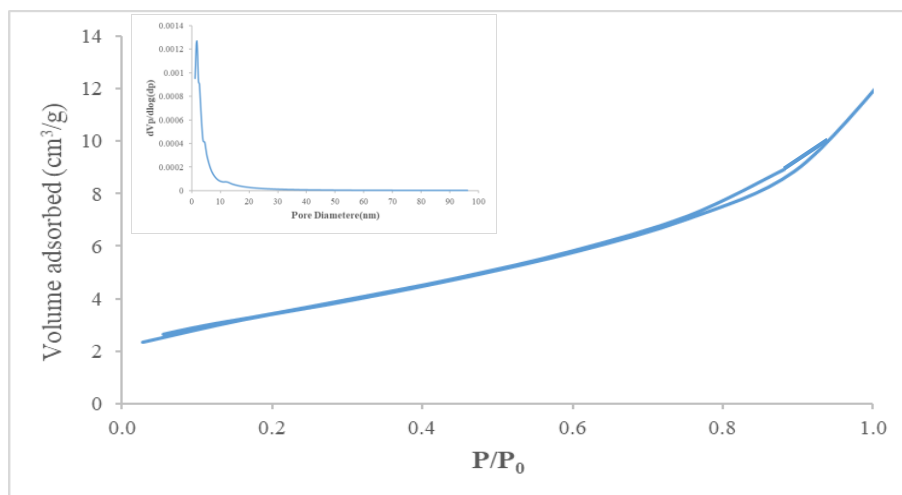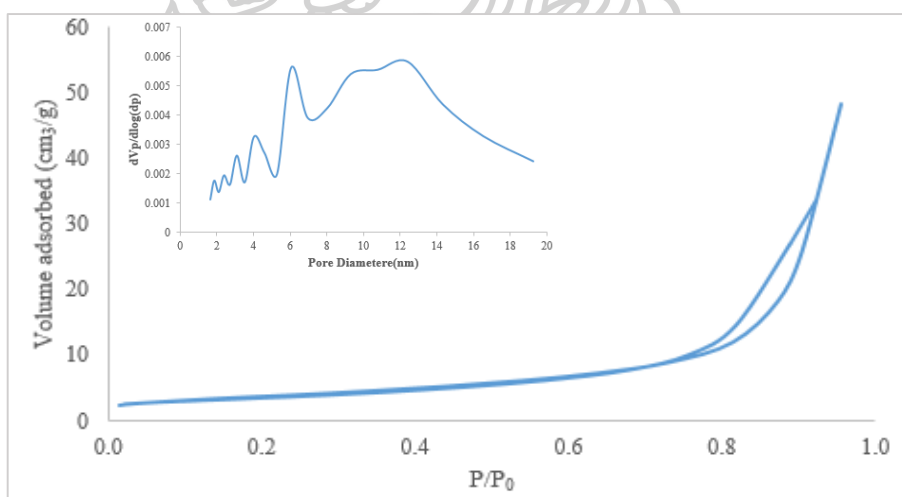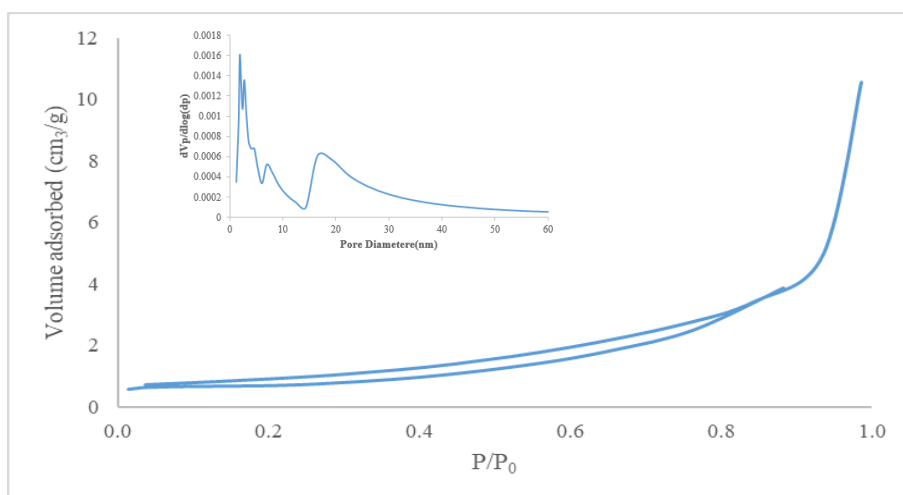
Figure C.11 The N$_2$ adsorption/desorption isotherms and the pore size distribution of the 2Ni/LaCuO$_3$catalysts
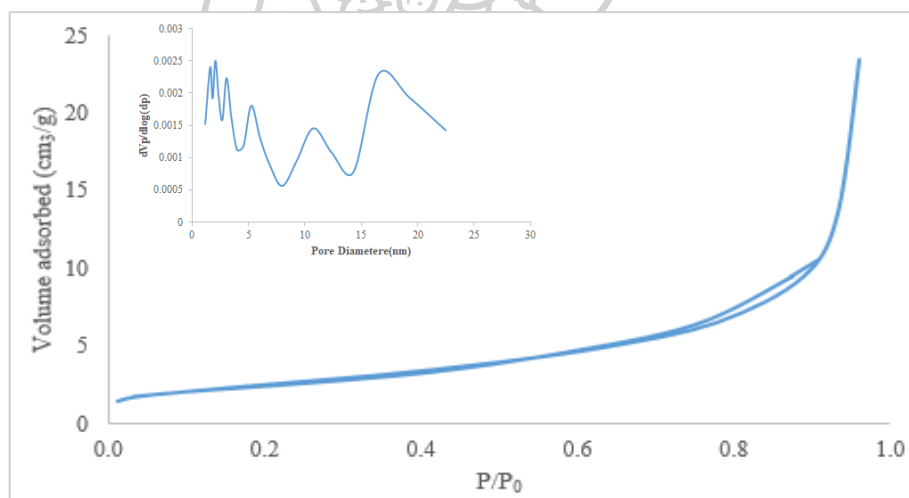
Figure C.12 The N$_2$ adsorption/desorption isotherms and the pore size distribution of the 2Ni/LaCuO$_3$catalysts

APPENDIX D

CALCULATION OF CH$_4$ AND CO$_2$ CONVERSION, H$_2$ YIELD AND H$_2$/CO

RATIO

The CH$_4$ and CO$_2$ conversions, H$_2$ and CO yield and H$_2$/CO ratio were calculated by equation as follows:

CH$_4$ Conversion (%)

$$= \frac{\text{mole of CH}_{4\text{in}} - \text{mole of CH}_{4\text{out}}}{\text{mole of CH}_{4\text{in}}} \times 100$$

CH$_4$ Conversion (%)

$$= \frac{\text{mole of CO}_{2\text{in}} - \text{mole of CO}_{2\text{out}}}{\text{mole of CO}_{2\text{in}}} \times 100$$

H$_2$ Yield (%)

$$= \frac{\text{mole of H}_{2\text{out}}}{2\text{mole of CH}_{4\text{in}}} \times 100$$

CO Yield (%)

$$= \frac{\text{mole of CO}_{\text{out}}}{\text{mole of CH}_{4\text{in}} + \text{mole of CO}_{2\text{in}}} \times 100$$

H$_2$/CO ratio

$$= \frac{\text{mole of H}_{2\text{out}}}{\text{mole of CO}_{\text{out}}}$$

They are defined as moles of CH_4, CO_2, H_2 and CO converted with the calibration curve in figure E. 2 with area of CH_4, CO_2, H_2 and CO gases from computer program based plot on TCD (GC-14B)

Figure E.2   Calibration curve of CH_4 (a), CO_2(b), H_2(c) and CO(d) gases

REFERENCES

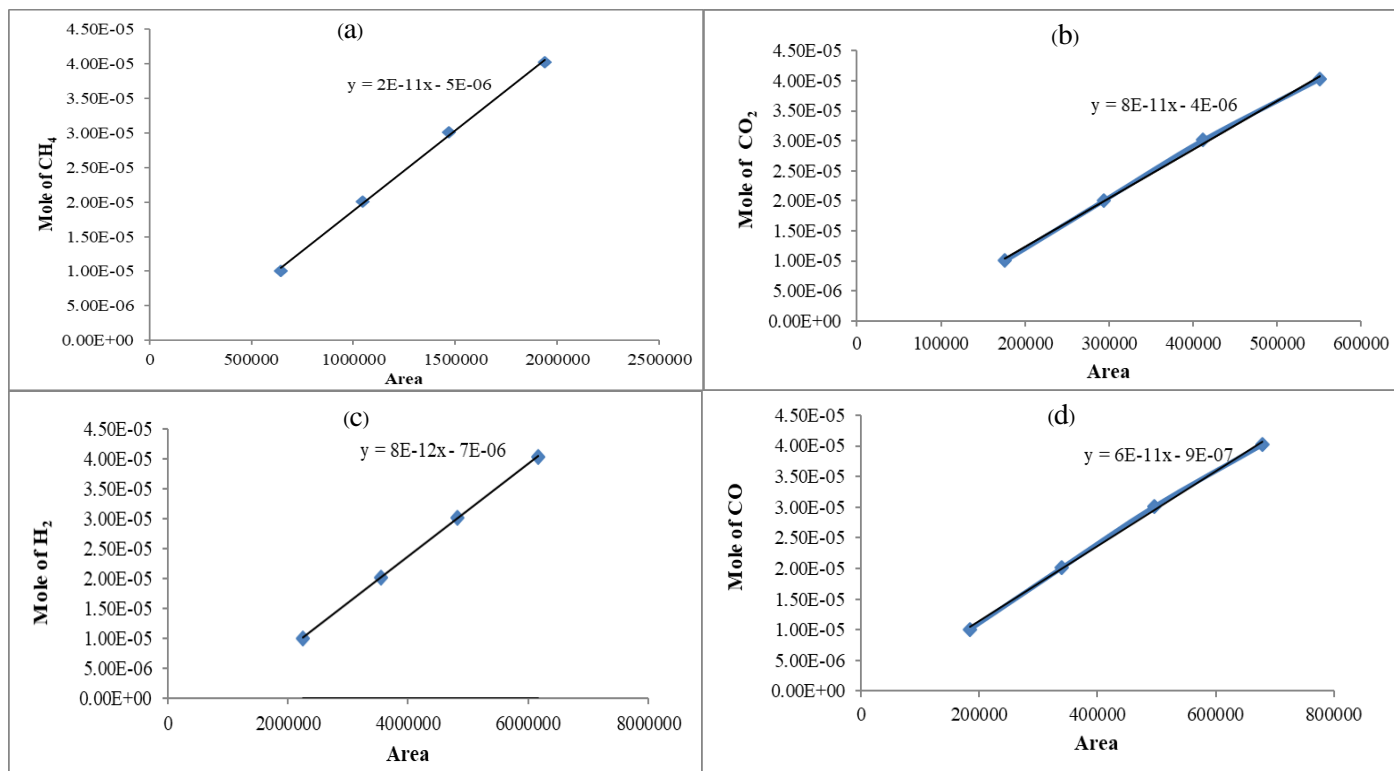1. Budiman, A.W., et al., *Dry reforming of methane over cobalt catalysts: a literature review of catalyst development.* Catalysis Surveys from Asia, 2012. **16**(4): p. 183-197.

2. Basile, A., et al., *Membrane reactors for energy applications and basic chemical production.* 2015: Elsevier.

3. Wang, S., G. Lu, and G.J. Millar, *Carbon dioxide reforming of methane to produce synthesis gas over metal-supported catalysts: state of the art.* Energy & Fuels, 1996. **10**(4): p. 896-904.

4. Abasaeed, A.E., et al., *Catalytic performance of CeO_2 and ZrO_2 supported Co catalysts for hydrogen production via dry reforming of methane.* International Journal of Hydrogen Energy, 2015. **40**(21): p. 6818-6826.

5. Jabbour, K., et al., *Characterizations and performances of Ni/diatomite catalysts for dry reforming of methane.* Chemical Engineering Journal, 2015. **264**: p. 351-358.

6. Ikkour, K., et al., *Activity of Ni substituted Ca-La-hexaaluminate catalyst in dry reforming of methane.* Catalysis letters, 2009. **132**(1-2): p. 213-217.

7. Valderrama, G., C.U. de Navarro, and M.R. Goldwasser, *CO_2 reforming of CH_4 over Co-La-based perovskite-type catalyst precursors.* Journal of Power Sources, 2013. **234**: p. 31-37.

8. Lu, Y., et al., *Influence of the synthesis method on the structure of Pd-substituted perovskite catalysts for methane oxidation.* Catalysis today, 2013. **208**: p. 42-47.

9. Galinsky, N., et al., *$Ca_{1-x}A_xMnO_3$ (A= Sr and Ba) perovskite based oxygen carriers for chemical looping with oxygen uncoupling (CLOU).* Applied Energy, 2015. **157**: p. 358-367.

10. Wu, Q., et al., *Fabrication of nanofibrous A- or B-sites substituted $LaCoO_3$ perovskites with macroscopic structures and their catalytic applications.* Materials Research Bulletin, 2014. **51**: p. 295-301.

11. Chiarello, G.L., et al., *Flame-synthesized $LaCoO_3$-supported Pd: 1. Structure, thermal stability and reducibility.* Journal of Catalysis, 2007. **252**(2): p. 127-136.

12. Valderrama, G., C.U. de Navarro, and M.R. Goldwasser, *CO_2 reforming of CH_4 over Co-La-based perovskite-type catalyst precursors.* Journal of Power Sources, 2013. **234**: p. 31-37.

13. Rivas, I., et al., *Perovskite-type oxides in methane dry reforming: Effect of their incorporation into a mesoporous SBA-15 silica-host.* Catalysis Today, 2010. **149**(3): p. 388-393.

14. Zhu, Q., et al., *Synthesis, characterization, and catalytic performance of $La_{0.6}Sr_{0.4}Ni_xCo_{1-x}O_3$ perovskite catalysts in dry reforming of coke oven gas.* Chinese Journal of Catalysis, 2015. **36**(7): p. 915-924.

15. Rossetti, I., C. Biffi, and L. Forni, *Oxygen non-stoichiometry in perovskitic catalysts: Impact on activity for the flameless combustion of methane.* Chemical Engineering Journal, 2010. **162**(2): p. 768-775.

16. Lu, Y., et al., *Methane abatement under stoichiometric conditions on perovskite-supported palladium catalysts prepared by flame spray synthesis.* Applied Catalysis B: Environmental, 2014. **144**: p. 631-643.

17. Buchneva, O., et al., *La–Ag–Co perovskites for the catalytic flameless combustion of methane.* Applied Catalysis A: General, 2009. **370**(1-2): p. 24-33.

18. Chiarello, G.L., et al., *Flame-synthesized LaCoO₃-supported Pd: 1. Structure, thermal stability and reducibility.* Journal of Catalysis, 2007. **252**(2): p. 127-136.

19. Chang, J.-S., et al., *Catalytic behavior of supported KNiCa catalyst and mechanistic consideration for carbon dioxide reforming of methane.* Journal of Catalysis, 2000. **195**(1): p. 1-11.

20. Lima, S., et al., *Structural features of La₁₋ₓCeₓNiO₃ mixed oxides and performance for the dry reforming of methane.* Applied Catalysis A: General, 2006. **311**: p. 94-104.

21. Valderrama, G., et al., *LaNi₁₋ₓMnₓO₃ perovskite-type oxides as catalysts precursors for dry reforming of methane.* Applied Catalysis A: General, 2018. **565**: p. 26-33.

22. Arora, S. and R. Prasad, *An overview on dry reforming of methane: strategies to reduce carbonaceous deactivation of catalysts.* RSC Advances, 2016. **6**(110): p. 108668-108688.

23. Usman, M., W.W. Daud, and H.F. Abbas, *Dry reforming of methane: Influence of process parameters—A review.* Renewable and Sustainable Energy Reviews, 2015. **45**: p. 710-744.

24. Nikoo, M.K. and N. Amin, *Thermodynamic analysis of carbon dioxide reforming of methane in view of solid carbon formation.* Fuel Processing Technology, 2011. **92**(3): p. 678-691.

25. Kathiraser, Y., et al., *Kinetic and mechanistic aspects for CO₂ reforming of methane over Ni based catalysts.* Chemical Engineering Journal, 2015. **278**: p. 62-78.

26. Al-Fatesh, A.S., A.H. Fakeeha, and A.E. Abasaeed, *Effects of selected promoters on Ni/Y-Al₂O₃ catalyst performance in methane dry reforming.* Chinese Journal of Catalysis, 2011. **32**(9-10): p. 1604-1609.

27. Sokolov, S., et al., *Effect of calcination conditions on time on-stream performance of Ni/La₂O₃–ZrO₂ in low-temperature dry reforming of methane.* International Journal of Hydrogen Energy, 2013. **38**(36): p. 16121-16132.

28. Ay, H. and D. Üner, *Dry reforming of methane over CeO₂ supported Ni, Co and Ni–Co catalysts.* Applied Catalysis B: Environmental, 2015. **179**: p. 128-138.

29. Wang, X., et al., *New route to CeO₂/LaCoO₃ with high oxygen mobility for total*

benzene oxidation. Applied Surface Science, 2017. **396**: p. 95-101.

30. Levy, M. R. , *Crystal structure and defect property predictions in ceramic materials.* 2005, University of London.

31. Royer, S., et al., *Perovskites as substitutes of noble metals for heterogeneous catalysis: dream or reality.* Chemical reviews, 2014. **114**(20): p. 10292-10368.

32. Rivas, M.E., et al., *Structural features and performance of $LaNi_{1-x}Rh_xO_3$ system for the dry reforming of methane.* Applied Catalysis A: General, 2008. **344**(1): p. 10-19.

33. Chawl, S.K., et al., *Production of synthesis gas by carbon dioxide reforming of methane over nickel based and perovskite catalysts.* Procedia Engineering, 2013. **51**: p. 461-466.

34. Chiarello, G., et al., *Solvent nature effect in preparation of perovskites by flame-pyrolysis: 1. Carboxylic acids.* Applied Catalysis B: Environmental, 2007. **72**(3): p. 218-226.

35. Mota, N., et al., *Hydrogen production by reforming of diesel fuel over catalysts derived from $LaCo_{1-x}Ru_xO_3$ perovskites: Effect of the partial substitution of Co by Ru (x= 0.01–0.1).* Journal of Power Sources, 2011. **196**(21): p. 9087-9095.

36. Phraewphiphat, T. , et al. , *Syntheses, structures, and ionic conductivities of perovskite-structured lithium–strontium–aluminum/ gallium–tantalum-oxides.* Journal of Solid State Chemistry, 2015. **225**: p. 431-437.

37. Barros, B. , et al. , *CO_2 reforming of methane over La_2NiO_4-αAl_2O_3 prepared by microwave assisted self-combustion method.* Applied Catalysis A: General, 2010. **378**(1): p. 69-75.

38. Wang, N., et al. , *A comparison study on methane dry reforming with carbon dioxide over $LaNiO_3$ perovskite catalysts supported on mesoporous SBA-15, MCM-41 and silica carrier.* Catalysis today, 2013. **212**: p. 98-107.

39. Bhavani, A.G., W.Y. Kim, and J.S. Lee, *Barium substituted lanthanum manganite perovskite for CO_2 reforming of methane.* ACS Catalysis, 2013. **3**(7): p. 1537-1544.

40. Lima, S. , et al. , *Structural features of $La_{1-x}Ce_xNiO_3$ mixed oxides and performance for the dry reforming of methane.* Applied Catalysis A: General, 2006. **311**: p. 94-104.

41. Yang, E.-h., et al., *The effect of promoters in $La_{0.9}M_{0.1}Ni_{0.5}Fe_{0.5}O_3$ (M= Sr, Ca) perovskite catalysts on dry reforming of methane.* Fuel Processing Technology, 2015. **134**: p. 404-413.

42. Gallego, G.S., et al., *Dry reforming of methane over $LaNi_{1-y}B_yO_{3\pm\delta}$ (B= Mg, Co) perovskites used as catalyst precursor.* Applied Catalysis A: General, 2008. **334**(1): p. 251-258.

43. Provendier, H. , et al. , *Dry reforming of methane. Interest of La-Ni-Fe solid solutions compared to $LaNiO_3$ and $LaFeO_3$.* Studies in surface science and

catalysis, 1998: p. 741-746.

44. Moradi, G., M. Rahmanzadeh, and F. Khosravian, *The effects of partial substitution of Ni by Zn in LaNiO₃ perovskite catalyst for methane dry reforming.* Journal of CO₂ Utilization, 2014. **6**: p. 7-11.

45. Haas, O., R. Struis, and J. McBreen, *Synchrotron X-ray absorption of LaCoO₃ perovskite.* Journal of Solid State Chemistry, 2004. **177**(3): p. 1000-1010.

46. Ayodele, B.V., et al., *Production of CO-rich hydrogen from methane dry reforming over lanthania-supported cobalt catalyst: kinetic and mechanistic studies.* international journal of hydrogen energy, 2016. **41**(8): p. 4603-4615.

47. Ao, M., et al., *Structure and activity of strontium substituted LaCoO₃ perovskite catalysts for syngas conversion.* Journal of Molecular Catalysis A: Chemical, 2016. **416**: p. 96-104.

48. Li, X., et al., *Dry reforming of methane over Ni/La₂O₃ nanorod catalysts with stabilized Ni nanoparticles.* Applied Catalysis B: Environmental, 2017. **202**: p. 683-694.

49. Albarazi, A., M.E. Gálvez, and P. Da Costa, *Synthesis strategies of ceria–zirconia doped Ni/ SBA-15 catalysts for methane dry reforming.* Catalysis Communications, 2015. **59**: p. 108-112.

50. Valderrama, G., C. Urbina de Navarro, and M.R. Goldwasser, *CO₂ reforming of CH4 over Co-La-based perovskite-type catalyst precursors.* Journal of Power Sources, 2013. **234**: p. 31-37.

51. Yang, E.-h., et al., *The effect of promoters in La₀.₉M₀.₁Ni₀.₅Fe₀.₅O₃ (M= Sr, Ca) perovskite catalysts on dry reforming of methane.* Fuel Processing Technology, 2015. **134**: p. 404-413.

52. Kathiraser, Y., et al., *Inverse NiAl₂O₄ on LaAlO₃-Al₂O₃: unique catalytic structure for stable CO₂ reforming of methane.* The Journal of Physical Chemistry C, 2013. **117**(16): p. 8120-8130.

53. Villoria, J., et al., *Zirconia-supported LaCoO₃ catalysts for hydrogen production by oxidative reforming of diesel: Optimization of preparation conditions.* Catalysis Today, 2008. **138**(3-4): p. 135-140.

54. Hammouda, S.B., et al., *Reactivity of novel Ceria–Perovskite composites CeO₂-LaMO₃ (MCu, Fe) in the catalytic wet peroxidative oxidation of the new emergent pollutant 'Bisphenol F': Characterization, kinetic and mechanism studies.* Applied Catalysis B: Environmental, 2017. **218**: p. 119-136.

55. Rivas, I., et al., *Perovskite-type oxides in methane dry reforming: Effect of their incorporation into a mesoporous SBA-15 silica-host.* Catalysis Today, 2010. **149**(3-4): p. 388-393.

56. Lukashuk, L., et al., *Operando XAS and NAP-XPS studies of preferential CO oxidation on Co₃O₄ and CeO₂-Co₃O₄ catalysts.* Journal of Catalysis, 2016. **344**: p. 1-15.

57.   Hueso, J.L., et al., *Structural and chemical reactivity modifications of a cobalt perovskite induced by Sr-substitution. An in situ XAS study.* Materials Chemistry and Physics, 2015. **151**: p. 29-33.

58.   Benrabaa, R., et al., *Sol–gel synthesis and characterization of silica supported nickel ferrite catalysts for dry reforming of methane.* Catalysis Communications, 2015. **58**: p. 127-131.

59.   Nair, M. M., S. Kaliaguine, and F. Kleitz, *Nanocast LaNiO₃ perovskites as precursors for the preparation of coke-resistant dry reforming catalysts.* ACS Catalysis, 2014. **4**(11): p. 3837-3846.

60.   Li, Y., et al., *Optical properties of La₂CuO₄ and La₂₋ₓCaₓCuO₄ crystallites in UV–vis–NIR region synthesized by sol–gel process.* Materials Characterization, 2012. **64**: p. 36-42.

61.   Hou, Y.-C., et al., *Ni-substituted LaMnO₃ perovskites for ethanol oxidation.* RSC Advances, 2014. **4**(11): p. 5329-5338.

62.   Touahra, F., et al., *Enhanced catalytic behaviour of surface dispersed nickel on LaCuO₃ perovskite in the production of syngas: an expedient approach to carbon resistance during CO₂ reforming of methane.* international journal of hydrogen energy, 2016. **41**(4): p. 2477-2486.
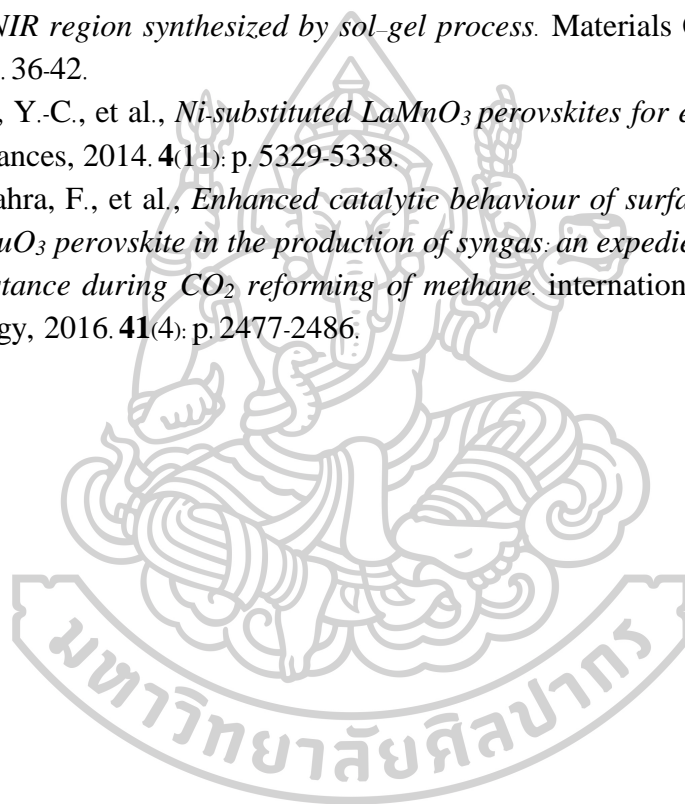
VITA

NAME	MissPhakampai Aunmunkong
DATE OF BIRTH	25 March 1987
PLACE OF BIRTH	Bangkok, Thailand.
INSTITUTIONS ATTENDED	Department of Chemical Engineering, Faculty of Engineering and Industrial Technology, Silpakorn University, Nakhon Phathom, Thailand.
HOME ADDRESS	House No.118, Village No.5, Watlamud sub-district, Nakhon Chai Si District, Nakhonpathom Province, Thailand, 73120.